The United Nations University

GEOTHERMAL TRAINING PROGRAMME
Orkustofnun, Grensásvegur 9,
IS-108 Reykjavík, Iceland

Reports 1999
Number 1

ASSESSMENT OF SCALING AND CORROSION PROBLEMS IN THE KEBILI GEOTHERMAL FIELD, TUNISIA

Mongi Elguedri
Ministry of Agriculture,
Regional Commissariat for Agricultural Development - CRDA Kebili,
Kebili 4200
TUNISIA

ABSTRACT

Severe scaling problems have been encountered in the pipeline networks in the low-temperature geothermal field in Kebili, South Tunisia, due to the chemical changes resulting from degassing, evaporation and cooling that are necessary to produce a valid water for oasis irrigation. Data from three wells: Kebili-Ras Elaïn-C.I.10, Om Somaa-C.I.5 and Lymagues-C.I.8 was analysed to study the calcium carbonate scaling potential. One scaling sample and two pipe samples from Kebili-Ras Elaïn pipeline network were also analysed for scale identification by microscope and X-Ray Diffraction. The scale consisted mainly of aragonite. Two chemical models, the WATCH program and the SOLVEQ program were used to predict calcite and aragonite scaling, and to determine the allowable supersaturation before calcium carbonate formation becomes a problem. The saturation index, log (Q/K), for the two calcium carbonate polymorphs are high. For calcite the log (Q/K) exceeds 1.50 and for aragonite at the final step log (Q/K) exceeds 1.30, which indicates that the $CaCO_3$ scaling problems will occur. Based on these findings more accurate predictions of calcium carbonate scaling can be made.

1. INTRODUCTION

Tunisia, the North-African country, has a total land area of 164,000 km^2 and about 9 million inhabitants. As a developing country the economy is mainly based on agriculture, tourism, and varied industrial activities. The country's arable lands are estimated at 5 million hectares and 340,000 hectares of land are irrigated. The main agricultural products are olive oil, dates, cereals and citrus fruits. Agriculture accounts for 22% of exports and provides work for 22% of the active population. Tunisia's water resource potential from precipitation and underground aquifers is 4,800 million cubic metres per year. Nearly 65% of the groundwater is being tapped at present.

The result of drawdown in the water level in wells utilising the medium aquifer (complex terminal) in the Kebili area provided information to the government on the possibility of utilising geothermal water from the deep aquifer (continental intercalaire). Since the beginning of the 1980's the government's policy was oriented to supplying oases in the south with geothermal water for irrigation. For this reason, more than 20 geothermal wells were drilled in the Kebili area with a resulting total flow rate of 1,100 l/s and a

temperature varying from 24 to 73˚C. In addition, in 1986, the government started to use the geothermal water for heating and irrigation of greenhouse farming.

Two designs are used for the oases irrigation pipeline network. The first one is to store the return water from greenhouses in plastic storage ponds. The water is produced during the heating of greenhouses at night, and then during the day transported by gravity to the oasis. The second one is to transport the water, from the geothermal wells through atmospheric cooling towers to the oases. The cooling towers are equipped with electric fans, but most of the time the water is cooled naturally by wind (120 days/year are windy) without any consumption of electricity.

After a few years of utilisation, scale formation was observed inside the supply pipeline from the cooling tower. Scale formation, which can take place in the reservoir as well as in the production, utilisation and reinjection facilities, is one of the major problems in geothermal operations. Depending on the chemical composition of the geothermal well fluids, different types of scales are found in various geothermal areas.

The presence of the calcium ion and bicarbonate alkalinity is common in almost every source. The relative insolubility of calcium carbonate is one of the most common causes of scaling. Calcium carbonate scaling problems have been reported in most of the countries using and developing geothermal resources.

Calcium carbonate scaling is often caused by the mixing of waters from different aquifers, but degassing of carbon dioxide because of lower pressure or evaporation by water-air contact in cooling towers, are the main reasons for calcium carbonate scaling. Understanding the mechanism of calcium carbonate formation and further, giving precise prediction information is very important in order to decide upon the type of scale prevention or scale removal methods. Based on thermodynamic and experimental studies, various calcium carbonate scaling prediction models have been developed.

In this report, the WATCH program (Bjarnason, 1994) and the SOLVEQ program (Spycher and Reed, 1989) are used to analyse the calcium carbonate scaling problem in the low-temperature utilisation network in Kebili area, South Tunisia.

2. GEOLOGY AND GEOTHERMAL RESOURCES IN TUNISIA

Tunisia is located in a strategic area at the intersection of several tectonic plates (African, European and Mediterranean). The structural framework is characterized by a transition between the Saharan platform in the southern part of Tunisia, and the alpine folded structures (Atlas domain and Tellian trough) in the northern part. According to the description of Ben Dhia and Bouri (1995), Tunisia is subdivided into five geothermal provinces (numbered PI - PV) as shown in Figure 1. The criterion used for this division is a relative geological and structural homogeneity for each region, with the presence and regrouping of hot springs. The Triassic and Jurassic outcrops are linked with major structural events (Zaghouan mountain, North-South Axis, North domain). Furthermore, a relatively good correlation could be established between these outcrops and the hot springs.

The geology of the Northwestern province (PI) is greatly affected by the overthrust of the alpine nappes, dated as upper Miocene, and the thick deposit of sandy layers “Nummedian formation”. The hottest springs occur with a discharge rate ranging between 5 and 40 l/s; there are also a few granitic and volcanic rock outcroppings (approximately 10 million years of age). This region is geologically related to the Toscan Italian province, and so is expected to be a potentially high-energetic zone. The geothermal potential of this region is assessed by data and investigative programmes which are rather superficial; aquifers of geothermal interest may occur within Triassic and Jurassic formations of the Hairech and Ichkeul mountains, including most of the hot springs. Provinces II and III constitute the “Atlas domain”, and are separated from province I by the “Diapirs zone”. Main structural features of the region show three major directions: N-S axis, SW-NE Atlas folds and NW-SE Quaternary grabens. Overlying the Triassic evaporities are thick sedimentary series with alternating limestones, shales and sandstones, from Jurassic,

Cretaceous and Tertiary formations with frequent lateral lithological variations. These rocks represent both marine and continental sedimentary facies and are investigated either by surface or subsurface surveys. Many layers of sands, sandstones and limestones have been defined as potential hydrothermal objectives. Province IV "chotts province" is structurally known as "Tebaga Anticline". This most important E-W structure in Tunisia constitutes a transition between the Atlas and the Saharan domain. Sedimentary, Jurassic and Cretaceous rocks represent the most particular occurring layers, especially early Cretaceous with more than 4000 m of sands and clays, constituting the extreme Northern part of the most important aquifer of the whole North African Sahara. The Southern province (PV) contains the biggest sedimentary basin in Tunisia, with the thickest and widest deep aquifer system. Numerous exploration oil wells have been drilled in this region, providing vast amounts of information on the underground layers. The province covers almost half of the country, with about 80,000 km^2 of predominately arid lands. The province is located in the Northern part of the stable Saharan platform. Tectonic features are dominated by the monoclinal trend of the present layers, dipping gently from east to west.

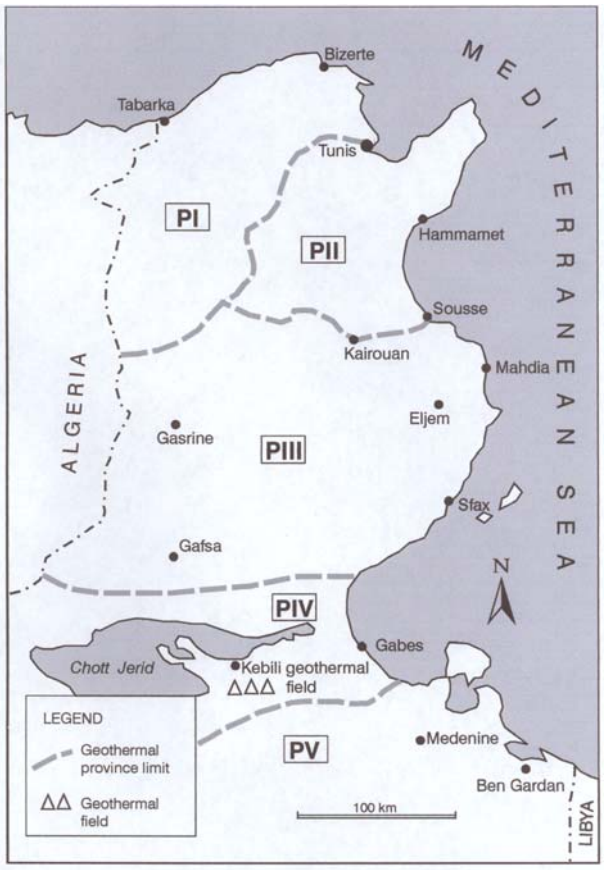

FIGURE 1: Geothermal provinces in Tunisia

2.1 Northern area

A complex geological setting, where volcanic rocks are more common than in the other regions, characterizes the northwest region (PI) with a high density of thermal manifestations. In this region, there are 28 hot springs with a low flow rate (less than 10 l/s) and high salinity (10 g/l). The hot springs are preferably associated with tectonic activity (faults and fissures). Two types of springs characterize this region, the first called Flysch Numidian and the second Atlasic Tectonic. The Flysch Numidian is a result of abnormal contact of Tertiary and Quaternary formations with old formations. The temperature of water in these springs exceeds 40˚C and some springs such as Hammam Bourguiba are above 50˚C. Based on a gradient of 33˚C/km, the water temperature in this aquifer is estimated to be 40˚C at 600 m depth and 65˚C at 1,360 m depth. Springs associated with Atlasic Tectonic are from deep levels and reach the surface through big faults. The most important springs are Hammam Zriba, Djebal Ouest, Hammam Lif and Kourbous. The temperature is always higher than 40˚C. The maximum temperatures predicted in this aquifer are 50˚C at 1,000 m depth and 65˚C at 1,500 m depth (Ben Mohamed, 1997).

2.2 Central area

The low Zerbag and the low Cretaceous, from Tertiary formations, are the two aquifers in this region. The low Zerbag is characterized by temperatures of 37-40˚C, a depth of 480-540 m and a salinity of 4.3 g/l. The low Cretaceous is characterized by temperatures of 39-51˚C, a depth of 1,300-1,800 m and a salinity of 3.3-9 g/l. The artesian exploitation flow rate is estimated to be 150 l/s.

2.3 Southern area

In South Tunisia the artesian flow rate from the hot springs is usually higher than from the northern part of Tunisia (Stefánsson, 1986). The gradient is approximately 21˚C/km. The aquifers are crossing from Atlasic Tectonic to the desert plate (Sahara) with a temperature of 20-75˚C. The Complexe Terminal (CT), the Djeffara and the Continental Intercalaire (CI) are the three main aquifers. Other formations with temperatures above 35˚C exist inside Prenien, Triassic and Jurassic rocks but have a salinity of 10-75 g/l. These formations are of interest for oil drilling.

The Complexe Terminal covers the regions of Nefzaoua (Kebili), Gafsa and Djerid (Tozeur). It has been exploited at relatively low depths for more than thirty years and contains low-enthalpy water which is characterized by a temperature ranging from 20 to 45˚C and well depths between 100 and 1,200 m. The salinity varies from 1 to 6.5 g/l. The total flow rate of this aquifer is estimated at 1,125 l/s of which 1,000 l/s are used (about 89%). The Djeffara covers the regions of Gabes and Medenine (southeast region of Tunisia). It is exploited at shallow depths (100-500 m) with a varying temperature of 21-29˚C and total flow rate of 1,100 l/s, which is all used. The Continental Intercalaire covers the regions of Nefzaoua, Djerid, Gabes and the extreme south and extends to Algeria and Lybia. It is characterized by temperatures ranging from 35˚ to 75˚C, well depth ranging from 1,200 to 2,800 m, a pressure of 14-22 bars and salinity of 2.2-4.2 g/l. Geothermal resources in this aquifer are evaluated at 3,200 l/s of which 91% is exploited. At present, the geothermal resource potential in the southern region of Tunisia is estimated at 5,500 l/s and 92% is exploited. The main data is summarized in Table 1.

TABLE 1: Hydraulic resources and exploitation in South Tunisia (Mamou, 1992)

Aquifers	Total resources (l/s)	Exploitation	
		(l/s)	(%)
Complexe Terminal (CT)	1,125	1,000	89
Djeffara	1,100	1,100	100
Continental Intercalaire (CI)	3,200	2,900	91
Total	5,425	5,000	92

3. DESCRIPTION OF THE UTILIZATION OF THE KEBILI GEOTHERMAL FIELD

The Kebili geothermal field is situated within the PIV geothermal province. The main aim of the geothermal utilization in Kebili was to supply the oases with water for irrigation after the excessive drawdown of the medium aquifer (complexe cerminal, CT) which was the only hydraulic resource for the oases. The drawdown was caused by over-exploitation. To stop the decrease in profitability due mainly to the use of electricity for pumping water from the medium aquifer wells, a programme was initiated to use geothermal water for irrigation. The different components of the hydraulic network are shown in Figure 2.

3.1 Geothermal wells

The geothermal resource tapped by the wells is the deep aquifer (continental intercalaire, CI) which is characterized by relatively hot water (30-75˚C) at a depth reaching 2,800 m. The resources at Kebili are estimated at 1,288 l/s by. From 1952 to 1999 a total of 33 wells were drilled in the region. The first well was drilled at Om Elfareth locality in 1952. The main period of drilling wells was in 1985 (six wells) and in 1986 (six wells). Then there was no drilling activity until 1991 when one well was drilled. In 1992 three wells were drilled, and another three in 1993. In 1994 three wells were drilled having a flow rate of 70 l/s each and three corresponding new oases (Douz Lazala CI.18, 70 ha, Souk Lahad CI.17, 30 ha, and

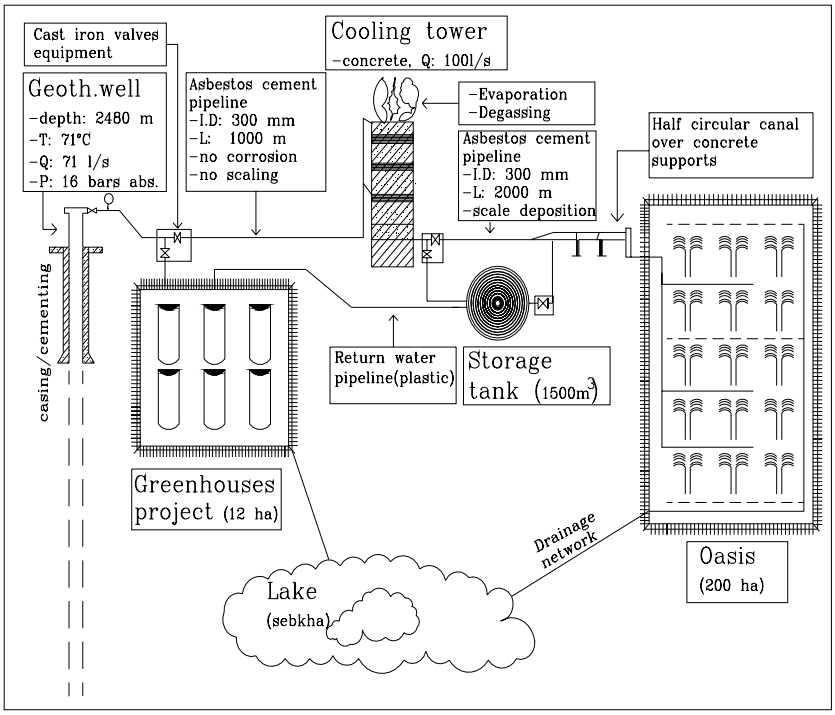

FIGURE 2: Schematic diagram of geothermal water utilisation in Kebili

Kebili- Bazma CI.16, 50 ha) were created in 1999. In 1999 another well was drilled at the Baheir area. Tables 2 and 3, respectively, show the physical and chemical data for the main wells which are connected to the atmospheric cooling towers.

The geothermal water is mainly used for agricultural purposes, irrigation of oases, heating and irrigation of greenhouses, but it is also utilized for hotels (swimming pools) and animal husbandry. The main uses of the water as a geothermal resource are as follows:

Swimming pools. Two pools at two different hotels at Douz are supplied with hot water from well CI.12 with a total flowrate of 16 l/s (8 l/s for each hotel). The return water from the hotels is used for irrigating the oasis surrounding them. The rest of the water is used for heating and irrigation of greenhouses. The temperature of the well is 53˚C. Another swimming pool is at Kebili-Ras Elaïn, supplied by well CI.10.

TABLE 2: Well data for 10 wells connected to the atmospheric cooling towers (CRDA, 1996)

Well name	Year	Temperature (˚C)	Pressure (bar-a)	Flow rate (l/s)	Depth (m)
Bouabdellah CI.4	1985	70	15	65	2,200
Om Somaa CI.5	1985	70.9	5.2	73	2,229
Menchia CI.6	1986	71	16.7	61	2,310
Steftimi CI.7	1986	72.5	14.3	52	1,987
Lymagues CI.8	1985	72.5	10.8	42	1,752
Om Elfareth CI.9	1986	68	9.6	50	1,621
Ras-Elaïn CI.10	1986	70.9	5.2	71	2,580
Jemna CI.11	1986	59	19.7	118	2,192
Douz CI.12	1986	53	11.8	20	2,080
Dbebcha CI.14	1992	71	16	71	2,480

TABLE 3: Chemical composition in mg/l of 10 wells connected to the atmospheric cooling towers, samples collected at wellhead (CRDA, 1996)

Well name	pH	Ca	Mg	Na	K	SO_4	Cl	HCO_3	NO_3	TDS	CO_2
CI.4	7.9	208.42	97	375	12	677	667	122	6.2	2,270	88
CI.5	8.0	188.38	105	388	55	562	567	293	16.74	1,840	211
CI.6	8.1	258.5	80	382	48	630	702	232	3.72	2,590	167
CI.7	8.1	210.4	103	354	45	690	677	183	1.86	2,440	132
CI.8	8.3	240	103	287	36	931	497	86	-	2,450	62
CI.9	8.3	220.4	130	414	50	816	753	238	2.48	2,670	172
CI.10	8.2	248.5	85	402	41	745	617	201	3.72	2,410	145
CI.11	8.2	250.5	73	598	42	792	876	256	3.72	2,870	185
CI.12	8.2	232.4	66	418	44	696	674	110	8.68	2,320	79
CI.14	8.0	228	145	265	28	816	568	123	-	2,160	89

Bathing. Three wells are used for bathing (Hammam), two of them at Menchia and Steftimi have low flow rates (6 l/s for each well). The return water is used for irrigating the surrounding oases. The third well CI.10 is at Kebili with a flow rate of 71 l/s from which 6 l/s are taken for bathing. The rest is distributed between the greenhouses and the oases of Ras-Elaïn and Souk Elbayez.

Animal husbandry. Two wells are used, one at Chareb giving 4 l/s, and another in Mahbes with 5 l/s.

3.2 Repression pipeline

Generally, this pipeline is made of asbestos cement pipes. The geothermal water is transported by the pipe and the flowrate is divided into two parts by cast iron valves. The first one is to transport the water for heating and irrigating the greenhouse project. The second one is for transporting water to the atmospheric cooling tower. Figure 2 shows the different parts of the hydraulic network. The pipeline size was calculated by the following formula of Lechapt et Calmon:

$$J = 1.601 \times Q^{1.975} / D^{5.25} \quad \textbf{(1)}$$

where J = Pressure loss in pipe [mm/m];
Q = Flow rate [m^3/s];
D = Inside diameter [m].

The selected diameter of the asbestos cement pipeline depends on the flowrate and, in general, ranges between 150 and 400 mm. The pipes are laid underground at an average depth of 1.20 m. In the buried repression pipeline from the well to the cooling tower, no corrosion or scaling has been observed. The contact between pipeline and soil results in a lowering of the temperature of 2-3˚C per 1000 m of length.

3.3 Greenhouse project

The greenhouse project is placed close to the geothermal well. The transportation of geothermal water for a long distance to a greenhouse project needs high capital investment and the long distance significantly increases the pressure loss in the pipe.

The topography of the site is an important parameter in which the level and the slope should be taken into consideration. The greenhouse project should be located at a higher level than the oasis (Said, 1997). This siting has several advantages, such as the circulation of return water from the greenhouse project is transported by gravity to the oasis without requiring pumping, and the disposal of the drainage water from the greenhouse project is transported by gravity to the lake.

3.4 Return water pipeline

The asbestos cement or plastic pipeline transports the water from the greenhouses to the storage pond. Because the water is circulated under pressure in the closed system through the greenhouse project, no scaling is observed in this pipeline.

3.5 Atmospheric cooling tower

Several cooling tower design configurations have been used in geothermal applications over the years with varying degrees of long-term success. In Kebili geothermal field, the cooling tower is made of reinforced concrete. It has a total height of about 30 m, and it is open to the wind direction, in order to cool the water naturally without much use of electric fans. The essential elements are: Fans to draw air into the tower, water distribution (nozzles, piping, basin) to spread out water, fill to mix water and air, and structure to support the overall device. Fill, the heart of a cooling tower unit, provides a means to maximising air and water contact as these fluids flow through the unit. Several wood stick types are laid over the fill encouraging water film formation to maximize surface area for air exposure per unit volume of water.

The electric fan is used when there is no wind, especially in summertime. Then the flow rate increases due to increased requirements for plant irrigation at the same time as the air temperature is higher. In the top of a cooling tower, where the water pours out of the nozzles, the dissolved CO_2 starts to escape from the water by degassing and evaporation. This lowers the temperature by 4-5˚C. The water is aired through the cooling tower, and the temperature decreases further to 20-30˚C causing oxidation reaction. The change in the water chemical state will be explained in detail in Chapter 4. The cooling tower is built on the highest point and near the oasis in order to dominate the irrigation area (transporting water by gravity) and minimize the length of the pipeline to the oasis.

3.6 Storage of return water

Heating of greenhouses is needed during the nights from November to April, while irrigating the oasis is operated during the day in the same winter months. Therefore, it is necessary to store the return water from the greenhouses in a storage pond during the night and sometime it also receives water from the cooling tower. The storage pond capacity should be at least equal to the volume of return water for 2 or 3 nights. In order to facilitate the water supply to the oasis, the storage should be placed at an elevated level, if pumps are not to be installed. It is built by excavation and lined with plastic material.

3.7 Supply pipeline

The water is transported from the cooling tower and storage pond to the oasis. In the 1980's an asbestos cement pipe was laid underground. After a few years scaling was observed, and several times, the pipe was totally obstructed. For this reason, it was necessary to clean the pipe by using a cleaning machine which is called "hydro-cureuse". This machine is equipped with a piston pump and a flexible hose which is inserted inside the pipe. The water is pumped at a high pressure in order to remove the scaling material, and it can clean about 50 m of pipe length in either direction from an open point on the pipeline. At present, if topography allows, a semi-circular concrete canal is installed which rests on reinforced concrete supports, and inside the oasis a reinforced concrete rectangular canal is built above ground. The open canals are preferred in order to make cleaning by manual work easier, to reduce scaling, and to decrease the water temperature further.

3.8 Oasis

The main type of plants grown in the oasis is the date palm which occupies first place in the agricultural activity of the region due to its social and economical interest. The date sector occupies third place in the total agricultural export of the country after olive oil and fishing. The oasis is irrigated with geothermal water and in some cases by mixing with the medium aquifer (complexe terminal) water. Soil salinity, which affects the growth of plants and their production, is caused by the utilization of geothermal water for oasis irrigation. In order to keep the water level below the plant roots and reduce the build-up of salinity of the soil, a drainage network is installed inside the oasis and the drainage water is transported to a lake (sebkha).

4. SCALING

4.1 General

Water is always in the process of dissolving or depositing solids-scale (incrustation, fouling, deposits etc.). At present we know that the extent of mineral scaling from water is not wholly dependent upon the water itself, or its dissolved ion content. The mechanism of mineral scales formation is dependent upon the degree of supersaturation of the water with respect to a particular mineral, the rate of temperature change and changes in the pressure as well as the pH of the water. Thus, where water is used, one can expect a variety of potential deposition problems. Water is a universal solvent, since almost everything is soluble in it to some extent. This fact, as well as definite solubility limits, results in water's ability to dissolve and deposit minerals. The solubility of a given mineral in water is controlled by variations in temperature, pressure, pH, redox potential and the relative concentrations of other substances in solution. The gas content of water can vary considerably due to its entry to the surface from an aquifer, the dissolution of water constituents and changes in pressure. An increase in the partial pressure of gases in water in turn may increase or decrease the mobility of some other constituents. Oxygen decreases the mobility of iron, while carbon dioxide increases the mobility of many constituents of which calcium is the most important. Hydrogen sulphide and carbon dioxide occur in variable amounts in geothermal waters. However, oxygen plays a significant role in the formation of iron compound deposits from geothermal waters in surface equipment. Natural waters commonly contain dissolved carbon dioxide gas. Large concentrations of carbon dioxide, particularly at the pressure encountered in deep wells, are converted to carbonic acid. This causes a decrease in the pH of the water. Iron is present in practically all rocks and is usually dissolved in groundwater in the form of bicarbonate. Upon exposure to air, soluble ferrous iron oxidizes to insoluble or colloidal ferric iron. A deposit that may undergo further oxidation is formed (Cowan and Weintritt, 1976).

4.2 Literature review

At each stage of the geothermal utilization process, the natural hydrothermal fluids that may have been at thermal and chemical equilibrium with heated reservoir rocks, can be exposed to substantial changes in temperature and pressure, which can affect the solubility of a variety of dissolved mineral species. The lowering of the fluid temperature can decrease the solubility of metal sulphide species and allow them to precipitate individually or together. For calcium carbonate the reverse is true, it is more soluble at a lower temperature. Changes in fluid pressure can allow a phase change to take place; it is either boiling or exsolution of dissolved gases. Loss of dissolved gases (carbon dioxide or hydrogen sulphide) from the geothermal water can also drastically affect the pH, and therefore the solubility of both calcium carbonate and sulphide minerals.

In intermediate and low-temperature geothermal systems calcium carbonate scaling has been reported by

many authors. Vuataz et al. (1989) dealt with calcite saturated waters in the sandstone aquifer at Melleray, France, where a combination of sulphide and calcite scale was responsible for the deterioration of reinjection well permeability. Kristmannsdóttir (1989) also notes that calcite scale has been encountered in low-temperature systems in Iceland when fluids are allowed to degas and, on occasion, when fluids of different temperatures, or salinities are allowed to mix. Prevention of scale deposition in low-temperature systems is typically controlled by limiting the extent of degassing and the resultant pH changes that bring about the supersaturation of carbonate minerals.

Mixed metal sulphide and oxide deposition has been reported in virtually every type of geothermal system including those of low and intermediate enthalpy. Criaud and Fouillac (1989) note that low-enthalpy fluids with high concentrations of dissolved solids can cause severe corrosion of steel production casings. The iron liberated by corrosion reacts rapidly with sulphide-rich geothermal fluids and causes higher deposition rates of metal sulphide scale than is typically found in higher temperature environments. Ungemach and Roque (1988) and Honegger et al. (1989) found that corrosion of mild steel production casing results in the deposition of large quantities of iron sulphide scale in both production and reinjection wells. The mechanism of corrosion attack has not been unequivocally identified, but theoretically possible processes include chemical attack by hydrogen sulphide and carbon dioxide, bacterial attack and galvanic attack.

The precipitation of dissolved solids from geothermal fluids is a virtually ubiquitous phenomenon, which takes place in geothermal fluids at a different chemical composition over a wide range of temperatures. Moreover, the precipitation of solids from natural fluids is a highly complex physical and chemical process that is still poorly understood and over which we have only limited control (Thomas and Gudmundsson, 1989).

Arnórsson (1989) reviewed theoretical considerations that apply to the deposition of calcium carbonate minerals from geothermal waters. Studies of geothermal fluid chemistry in different parts of the world indicate that the waters at depth in the reservoir are very close to being calcite saturated. Figure 3 shows the state of calcite saturation for selected Icelandic geothermal waters. Calcite undersaturation may exist in some fields, probably due to an insufficient supply of carbon dioxide to the system.

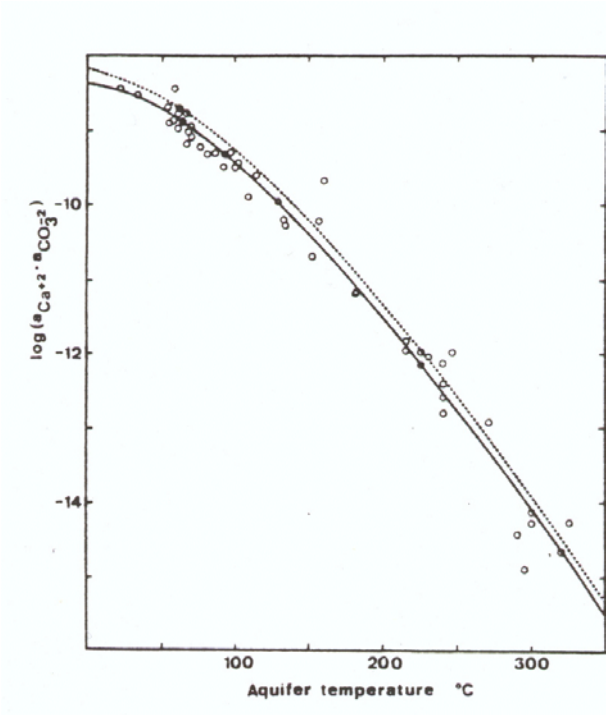

FIGURE 3: The state of calcite (solid line) and aragonite (broken line) saturation in selected Icelandic geothermal well waters (Arnórsson,1989)

Arnórsson (1978) has described in detail the changes that accompany the boiling of geothermal waters with respect to the state of calcite saturation. The degassing of carbon dioxide leads to an increase in pH and a strong increase in carbonate ion concentration. It is mostly this latter increase that is responsible for making an initially calcite saturated geothermal water supersaturated through boiling. If boiling is adiabatic the degree of supersaturation usually reaches maximum after cooling by 10-40˚C. The saturation is at maximum when boiled water has been almost quantitatively degassed with respect to carbon dioxide. Further boiling which leads to the cooling of the water will cause successively decreasing supersaturation because the solubility of calcite increases with decreasing temperature. For this reason calcite deposition can form a tapered plug as it is only deposited over a short section of pipe, e.g. inside well casings.

4.3 Chemistry of calcium carbonate deposition

Calcium carbonate is a polymorphous mineral and exists in several modifications. The two polimorphs commonly formed in nature are calcite and aragonite. Vaterite is a metastable form which crystallizes at ordinary temperatures and pressures. The solubility of the carbonate minerals is strongly influenced by the pH and the activity of the carbon dioxide dissolved in geothermal waters. At any given temperature, the solubility of calcite in solutions in equilibrium with a vapour phase increases with increasing carbon dioxide concentration up to about 1 mole carbon dioxide per kg (Miller, 1952). In solutions held at a constant total pressure, the solubility increases with increasing carbon dioxide concentration up to about 1 mole/kg and then decreases toward higher carbon dioxide concentrations (Sharp and Kennedy, 1965). At any given carbon dioxide pressure in the vapour phase, the solubility of calcium carbonate decreases with increasing temperature (Ellis, 1959):

Calcite: $$\log K_c = -171.9065 - 0.077993\,T + 2839.319/T + 71.595\log T \quad \textbf{(2)}$$

Aragonite: $$\log K_a = -171.9773 - 0.077993\,T + 2903.293/T + 71.595\log T \quad (3)$$

Vaterite: $$\log K_v = -172.1295 - 0.077993\,T + 3074.688/T + 71.595\log T \quad (4)$$

Calcite: $$\log K_c = 10.22 - 0.0349\,T - 2476/T \quad (5)$$

Equations 2-4 are from Plummer and Busenberg (1982), and Equation 5 from Arnórsson et al. (1982). The equilibrium constants of calcium carbonate as a function of temperature are calculated from the above equations at selected temperatures and listed in Table 4 and shown in Figure 4.

TABLE 4: Equilibrium constants for calcium carbonate at selected temperatures

Temperature		Log K_c (Calcite)	log K_a (Aragonite)	log K_v (Vaterite)
°C	K			
0	273.15	-8.38	-8.22	-7.74
20	293.15	-8.46	-8.31	-7.87
40	313.15	-8.62	-8.45	-8.05
60	333.15	-8.84	-8.64	-8.28
80	353.15	-9.12	-8.88	-8.55
100	373.15	-9.44	-9.17	-8.86
120	393.15	-9.80	-9.50	-9.21

Calcium carbonate precipitates can form in geothermal waters by the combination of calcium ions with carbonate ions. The calcite scales form very rapidly once the thermodynamic conditions of supersaturation are correct. For practical purposes the calcite kinetics can be assumed to be instantaneous. The loss of carbon dioxide and the associated pH increase are the principal causes for calcite precipitation. Calcite solubility decreases as the temperature increases from 25 to 100˚C and the solubility product continues to decrease up to 250˚C. However, the potential pressure of carbon dioxide at moderate to high pressure in a geothermal reservoir enhances its solubility. The solubility of calcite, aragonite (and other calcium carbonate minerals) may be expressed by the following reaction:

$$CaCO_{3,s} + 2\,H^+ = Ca^{+2} + CO_2 + H_2 \quad (6)$$

with the equilibrium constant being

$$\frac{(Ca^{+2})}{(H^+)^2} \times P_{CO_2} = K' \quad (7)$$

Parentheses indicate activity. The ratio of $(Ca^{2+})/(H^{+})^2$ in geothermal water tends to vary with temperature, the reason being that it is controlled by some mineral buffer. It is evident that this buffer, together with calcite, will fix P_{CO2} at any temperature and pressure. Dissolution or precipitation of the $CaCO_3$ phases calcite or aragonite can be written as the following reaction:

$$CaCO_{3,s} + CO_2\,(aq) + H_2O = Ca^{+2} + 2\,HCO_3^- \quad (8)$$

Aqueous CO_2 will be in equilibrium with CO_2 vapour if a gas phase is present. A movement of CO_2 from the liquid to the gas phase will result in decreasing the concentration of aqueous CO_2 and will drive Reaction 8 to the left. CO_2 loss from solution, therefore, results in precipitation of $CaCO_3$. A parallel reaction is:

$$CO_2\,(aq) + H_2O = H^+ + HCO_3^- \quad (9)$$

Loss of aqueous CO_2 to the gas phase will drive Reaction 9 to the left and the pH of the solution will rise.

As can be seen from Reaction 8 a certain supply of CO_2 is required to maintain sufficiently high CO_2 partial pressure for calcite saturation. The solubility of calcium carbonate minerals in an aqueous solution at any particular temperature increases with increasing partial pressure of CO_2. The degassing of CO_2 leads to an increase in pH and a strong increase in carbonate ion concentration. It is mostly this latter increase that is responsible for making initially calcite-saturated geothermal water supersaturated through boiling. However, dissociation of calcium-bearing ion pairs, particularly $CaSO_4$, as water temperatures decreases may also contribute to the extent of supersaturation.

Siliceous scaling is not common by exploitation of low- to medium-temperature water. The precipitation of silica normally does not occur until supersaturation with respect to opaline silica is reached and in low-temperature waters this does not happen at the temperatures prevailing in the hitaveitas (municipal heating services in Iceland). The silica may be deposited and form stains in wash basins and by leaky connections and faucets. This, however, is due to the evaporation of the water that leaves the minerals behind.

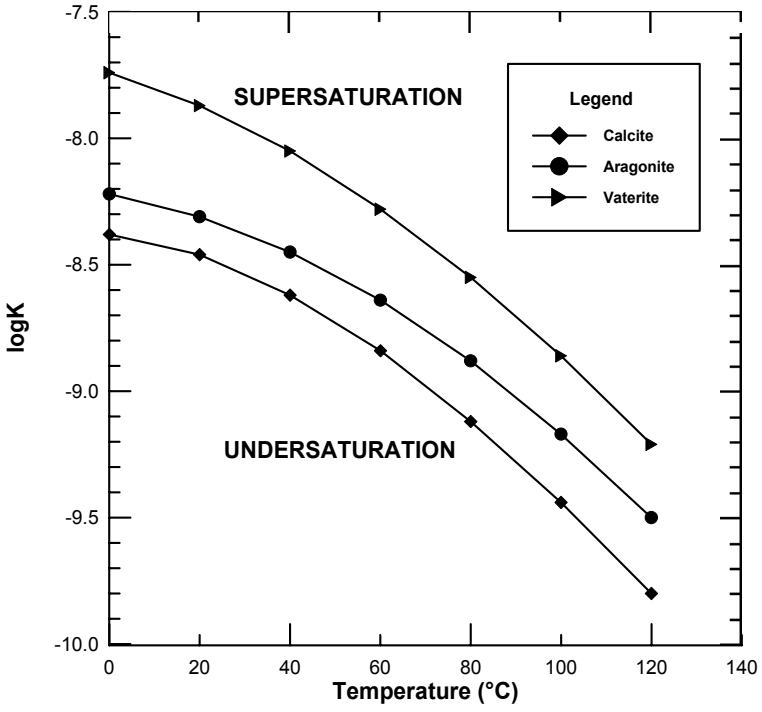

FIGURE 4: Solubility product, log K, for aragonite, calcite and vaterite based on the aqueous models (data from Plummer and Busenberg, 1982; Arnórsson et al., 1982)

Precipitation of other silicates is not common either. Mixing of fresh water into geothermal water may induce scaling by magnesium silicates. Magnesium concentrations in fresh water are generally much higher than in geothermal water. An exception is carbonate water where magnesium concentration can be quite high. Due to the inverse temperature dependence of magnesium silicate solubility, there is a great risk of their precipitation when fresh water is heated. The temperature and degree of de-aeration, together with the pH, are the controlling factors for supersaturation. Precipitates from a mixture of geothermal and fresh water from the Reykjavik heating system show more complicated XRD-patterns than those from heated cold water.

Special circumstances have given rise to scaling by hydrated zinc silicate, hemimorphite ($Zn_4(OH)_2Si_2O_7H_2O$) and also willemite (Zn_2SiO_4). This kind of scaling has formed in brass knees in copper pipes and in galvanized steel pipes. Scales of metal sulphides and oxides may occur in combination with metal corrosion in pipes and plant installations. As most metal sulphides are poorly soluble, such scale can be found in most metal pipes. Copper will be severely corroded in water containing hydrogen sulphide and subsequently copper sulphide will be precipitated. Iron sulphide, FeS_x will normally be deposited inside steel pipes carrying hydrogen sulphide water.

4.4 Prediction of calcite and aragonite scaling

Calcium carbonate which has three known naturally occurring polymorphs, calcite, aragonite and vaterite, is the most common scaling in geothermal production systems utilizing water of low and medium temperature. Where a potential scale problem exists it is obviously desirable to be able to predict its extent. Analysis of produced waters may tell us what can be expected throughout the rest of the system. There are several mathematical approaches available for predicting the scaling tendencies of geothermal water. WATCH (Bjarnason, 1994) and SOLVEQ (Spycher and Reed, 1989) are used in this report for interpreting the chemical composition of geothermal fluids. The two programs compute the chemical composition of downhole or aquifer fluids from chemical analysis of water, gas and steam condensate samples collected at the surface. The program output includes the pH, aqueous speciation, partial pressure of gases, redox potentials and activity products for mineral dissolution reactions.

The WATCH program can also be used to compute the concentrations of resulting species, activity coefficients, activity products and solubility products when the equilibrated fluid is allowed to cool conductively, or for adiabatic boiling from the reference temperature to some lower temperature. This is particularly useful in the study of scaling (Stanasel, 1996).

If the chemical composition of the fluid is known it is easy to find the saturation index (activity product) by using the WATCH or SOLVEQ programs. An expression of this, the saturation index, is used to predict scale formation:

$$SI = \log (Q / K) \tag{10}$$

The tendency for mineral precipitation or dissolution is indicated by comparison of K, the equilibrium constant (theoretical solubility product), to the function Q, the quotient of activities of species in solution (the ionic activity) of the respective minerals. The log Q and log K are calculated by using the WATCH and SOLVEQ programs. Also, log Q/K is calculated by using SOLVEQ program.

The method used to calculate the dissolution of $CaCO_3$ in the thermodynamic models relies on the reaction

$$CaCO_3 = Ca^{+2} + CO_3^{-2} \tag{11}$$

Reaction 11 is an acceptable substitute for Reaction 8, if the assumption is made that CO_3^{-2} and HCO_3^- are always in equilibrium with aqueous CO_2.

Calculations of composition and speciation of the geothermal water in the reservoir by using of the WATCH or SOLVEQ programs, can show if there is a general equilibrium in the water at the estimated reservoir temperature, if mixing of different aquifers has occurred, or an inflow of cold water. Changes in the water by cooling, boiling or other processes within the system can be modelled and subsequent changes in chemistry evaluated. This is an important tool for the assessment of production characteristics of the water. Changes in geothermal water over time are also clearly seen by comparing the changes in mineral equilibrium in water samples from different times.

It is common practice (Reed and Spycher, 1984) to calculate and plot against temperature the log Q/K

values, for various minerals likely to govern the chemistry of the water. When Q < K the saturation index is negative and the solution undersaturated with respect to the mineral considered. When Q > K the solution is supersaturated, and when Q = K the solution is exactly saturated or in equilibrium with the respective mineral. If the water is in equilibrium most of the curves will intersect the saturation line (log Q/K=0) at almost the same temperature. If there occur two or more main intersections, the fluid is likely to have reequilibrated at lower temperature, still keeping memory of an equilibrium at higher temperature.

The scaling potential is estimated by calculating log Q/K. A positive value for the relative log solubility of a mineral means that the solution is supersaturated with respect to that particular mineral and theoretically it would start to precipitate. However, experience gained in different fields utilizing geothermal water shows that minerals normally do not start to precipitate as soon as the solution becomes supersaturated. Production data for low-temperature geothermal waters in Iceland show, for example, that calcite normally does not start to precipitate until log Q/K value reaches 0.3-0.5 (Bai Liping, 1991).

4.5 Prevention of calcite and aragonite scaling

Effective scale prevention in geothermal operations is often critical to the success of a project. Unfortunately, scale prevention methods must be designed to very site-specific conditions of the field. These conditions dictate the type of scale prevention method or scale removal operation that will be feasible. Calcium carbonate scaling may be prevented by the following operations:

- Keeping the fluid under pressure, e.g. by pumping, to avoid degassing;
- Acting on carbon dioxide partial pressure;
- Acting on the pH of the solution;
- Using chemical additives (scale inhibitors);
- Cooling the fluid under pressure;
- Magnetic water treatment (experimental).

Pressure and temperature manipulations of the geothermal fluid can be achieved quite easily by pumping a geothermal well instead of relying on its natural flow. Utilizing a downhole pump will drastically decrease or eliminate the in-hole pressure and temperature drops caused by flashing. The produced fluids can be maintained as a single phase system by means of a mechanical downhole pump. Thus, the formation of "pressure sensitive" scaling such as calcite and aragonite can be eliminated. Another potential scale prevention method entails artificially maintaining a high carbon dioxide partial pressure by reinjecting some of the produced carbon dioxide back into the producing well, but it appears to work only for fluids with low carbon dioxide partial pressure.

Manipulation of the chemical composition of the geothermal fluid, particularly its pH, is another potentially valuable way to avoid scaling. Adding HCl to the geothermal fluid in order to decrease the pH below a certain value at which no calcite scaling can form is technically possible but rather expensive.

The utilization of scale inhibitors is the most common and promising method of combatting scaling problems. The main problem is to select the most suitable inhibitor among the many different chemicals on the market.

5. CORROSION

Corrosion means the destruction of a metal by chemical or electrochemical action of the surrounding environment. It is well known that iron and ordinary unalloyed steels corrode easily into rust. The most common case of corrosion is wet corrosion. The corrosive processes are very complex and take place in widely differing conditions (Hayashi, 1988).

The corrosive effects of a geothermal fluid on metals depend upon the chemical composition of that fluid. Geothermal waters have a wide range in composition, from strongly acidic waters containing sulphur and halogen acids which actively corrode most common alloys, to the more usual neutral-pH waters, which may lay down protective scales of calcite or metal oxides.

Contamination of geothermal fluids with oxygen (by aeration) drastically accelerates the surface corrosion of most alloys (Janik, 1985). The loss of dissolved gases is usually beneficial from a corrosion standpoint since the loss of carbon dioxide will tend to raise the pH in many geothermal waters. Corrosive attack on steel is reduced as the pH rises. Atmospheric gases can dissolve in the geothermal water if it is exposed to the atmosphere (in the cooling tower, for example). The only gas of any corrosive consequence is oxygen. Although the solubility of oxygen decreases to a minimum as the temperature rises near 100˚C, it is very important to exclude oxygen contact with geothermal water (Kindle et al., 1984).

5.1 Type of corrosion

This part of the report is based on the paper of Hayashi (1988). Generally speaking, we can find all the different types of corrosion in geothermal equipment and it is useful to recall the main characteristics of each.

Uniform or general corrosion is a general all-over attack on the metal surface that is transformed into rust. Uniform corrosion is often promoted by chloride or hydrogen ions. This type of corrosion is not of great concern because the lifetime of equipment can be accurately estimated on the basis of simple tests.

Pitting is a localized form of attack in which pits develop in the metal surface. Pitting is often associated with the breakdown of a passivation film or surface scale. High concentrations of chloride and hydrogen ions stimulate the dissolution of most metals. For the initiation of the pitting corrosion the rate of metal dissolution needs to be momentarily high at one particular point. Among the many factors that affect resistance to pitting, the following shall be discussed in greater detail. The only thing that can be said in general for all stainless steels is that the region pH above 12 is relatively risk free. Laboratory experiments with conventional 18/8 steel have shown that a 4 % NaCl solution provides the most frequent and deepest pits at pH between 4 and 8. The cathodic reaction occurring in conjunction with this pitting is considered to be the reduction of oxygen to hydroxyl ions. This means that the presence of oxygen is one absolute condition for the initiation of pitting. Oxygen, which has passivating properties against general corrosion, can thus be the direct cause of damage in an environment containing chloride ions. On the other hand, the attack is rapidly accelerated if oxygen is present, since it acts as a cathodic depolarizer. Pitting, just as all electrochemical corrosion, is hastened by elevated temperatures. However at atmospheric pressure a temperature rise to above about 80˚C can have a secondary effect involving a reduction in the intensity of pitting due to the fact that the content of dissolved oxygen is reduced because of its reduced solubility. Note, however, that this does not apply in systems kept under pressure.

Crevice corrosion is similar to pitting in that it is a localized attack. It occurs in crevices of equipment or under scale deposits. Contact between metal and nonmetal surfaces can cause crevice corrosion. Deposits such as corrosion products and scale deposits may produce crevice corrosion. As corrosion proceeds, oxygen within the crevice is consumed. Both chloride and hydrogen ions accelerate the dissolution of iron.

Stress corrosion cracking (SCC) is a type of failure promoted by a combination of the action of specific chemicals, such as chloride ion, and tensile stress. The presence of oxygen and increased temperatures increase the severity of attack. This is the most dangerous form of corrosion in geothermal environments. The most common agents that cause stress corrosion cracking are hydrogen sulphide and chloride. Aqueous solutions containing large amounts of hydrogen sulphide cause a form of stress cracking in 18/8 steel at low pH, especially below pH=4. Stress corrosion cracking caused by hydrogen sulphide is transcrystalline. This form of corrosion takes place primarily at low temperatures. At higher temperatures the solubility of hydrogen sulphide in water decreases in open systems. Oddly enough, this susceptibility

is also less in a closed, pressurized system at, for example, 120˚C. One possible explanation is that protective sulphide films are formed on the steel surface.

Sulphide stress cracking is a form of corrosion that may occur due to tensile stress and environments involving hydrogen sulphide in an aqueous phase. Low pH greatly accelerates material failure. Hydrogen blistering which may occur in low strength steels exposed to water containing hydrogen sulphide is similar. Sulphide stress cracking decreases in severity with increased temperature.

Other types of corrosion include galvanic corrosion, corrosion fatigue and exfoliation, which involve the formation of layers of corrosion products, but these are less important in geothermal systems.

5.2 Key corrosive species

Once the geothermal water is available for use, two important technological problems confront us, i.e. the prevention of scaling and corrosion. Silica and calcite and sometimes sulphide are the most important scales. Corrosive products are a second source of scale forming species. Both these sources of scales are important because of the adverse effect of scale on heat transfer and pumping efficiency (production or reinjection).

The species that are of greatest interest in geothermal water in relation to corrosion are hydrogen ion, chloride ion, hydrogen sulphide, carbon dioxide, oxygen and iron (see also Table 5).

TABLE 5: Principal effects of the main corrosive species

Species	Effects
Oxygen	Concentrations above 50 ppb cause pitting
pH	Corrosion rate decreases above pH =8
Carbon dioxide	Lower pH, increases corrosion
Hydrogen sulphide	Cathodic poison, promotes SSC
Temperature	Increase accelerates damage
Chloride ion	Promotes SCC and general corrosion

Hydrogen ion. The corrosion rate of most materials increases as pH decreases. The susceptibility of steels to stress corrosion cracking increases with increasing hydrogen ion concentration (lower pH). The main types of corrosion are pitting, crevice and stress corrosion cracking. The pH is a particularly significant characteristic of well water. A value of 6.5 or below, in water with a high carbon dioxide concentration (e.g. 20 mg/l) indicates that acid attack and direct hydrogen evolution are likely to occur, if the water is in contact with iron or steel. Higher pH values (above 8) are usually associated with water that causes localized pitting instead of general corrosion, particularly if dissolved oxygen is present, and such water may also scale well parts with carbonate deposits. Generally speaking, the lower the pH, the more corrosive the water is to iron well construction materials.

Chloride ion. This ion causes local breakdown of passive films. Uniform (general) corrosion can also increase with chloride ion concentration, but this action is generally less serious than local forms of attack. It is known that 5-10 ppm of chloride ion in the presence of oxygen may be sufficient at temperatures higher than 50˚C to promote stress corrosion cracking in stainless steel. A high chloride concentration causes increased solubility of iron in geothermal water by forming highly soluble complexes with the ferric ion.

Hydrogen sulphide. Probably the most severe effect of hydrogen sulphide is its attack on Cu and Ni alloys. The effect of hydrogen sulphide on iron compounds is less predictable. Accelerated attack occurs in some cases and inhibition in others. High-strength steels are often subject to sulphide stress cracking.

Oxidation of hydrogen sulphide in aerated geothermal process streams increases the acidity of the stream. Hydrogen sulphide is ubiquitous at the parts per million or parts per billion levels in geothermal waters. A low concentration may have a seriously detrimental effect especially if oxygen is also present. General corrosion by hydrogen sulphide in geothermal water proceeds in such a way that iron is oxidized to soluble ferrous iron at the anode, and hydrogen sulphide dissociates into hydrosulfide and sulphide ions at the cathode. The threshold concentration for attack is less than 30 ppb hydrogen sulphide. The presence of hydrogen sulphide in geothermal water, like the presence of iron, indicates a reducing water capable of dissolving iron. In addition, it indicates the presence of a sufficient concentration of hydrogen sulphide to corrode iron and steel significantly through direct combination with the metal and development of secondary corrosive cells. When hydrogen sulphide in low-temperature water is detected, there is reason to suspect the presence of sulphide-reducing bacteria. These can cause troublesome and very persistent localized pitting in addition to the general sulphide attack. Hydrogen sulphide concentrations of 0.5 ppm or more can damage certain copper alloys.

Carbon dioxide. Carbon dioxide is a mild oxidizing agent that causes increased corrosion of steel. However, the primary effects of carbon dioxide in geothermal systems involve carbonate species and pH changes. In acidic solutions, carbon dioxide can accelerate the uniform corrosion of carbon steels. The pH of geothermal water is largely controlled by carbon dioxide. On the other hand, bicarbonates and carbonates can display mild inhibitive effects. Carbon dioxide occurs naturally in many geothermal waters and has a major corrosive effect on steels. Theoretical considerations show a very high uniform corrosion rate in the presence of carbon dioxide and sodium chloride up to about 80˚C. At higher temperatures stable iron carbonate films, which slows the corrosion rate compared to predicted values, are formed. Carbonic acid itself is also believed to provide for an alternative cathodic half-reaction which yields bicarbonate ions and hydrogen.

Oxygen. Oxygen is present in low concentrations in most geothermal water. On the other hand, the inadvertent intrusion of even traces of this gas into geothermal water has lead to greatly accelerated corrosion. The simultaneous occurrence of oxygen and chloride can cause failure due to stress corrosion cracking. The addition of minor quantities of oxygen to a geothermal system can greatly increase the chance of severe localized corrosion of normally resistant metals. The corrosion of carbon steels is sensitive to trace amounts of oxygen. With low concentrations of hydrogen sulphide, dissolved oxygen from the air may persist in low-temperature geothermal water for some minutes, because of slow reaction kinetics. Preventing oxygen contamination is extremely difficult, especially if pumps other than downhole submersibles are used to move the geothermal water. The geothermal water may come into contact with the atmosphere (during reinjection) or oxygen might be one of the natural components in a gas accompanying the geothermal water. Aerated water causes a tenfold or greater increase in the uniform corrosion rate. Together with chloride ion, oxygen can initiate stress corrosion cracking at a certain temperature. It is very important to avoid oxygen contamination in the reinjection line at those points where the temperature may increase when the water flows into the injection wells. The corrosion of steel in aerated water is controlled by the reduction of dissolved oxygen on an iron-oxide covered surface and dissolution of iron under occlusions on the surface. Only a few ppb of oxygen in hot water is needed to cause localized corrosion and pitting. Even small amounts of oxygen can cause extensive corrosion damage. At low oxygen levels, the corrosion products are mainly iron sulphides (pyrite, pyrrhotite). As the oxygen level increases, magnetite becomes the major product.

Dissolved iron. The presence of heavy reddish-brown iron oxide stains in well discharge indicates an anaerobic well water, i.e. a reducing environment, capable of dissolving iron from both the aquifer rock and the steel well parts. In addition to its power to corrode, such water may also cause troublesome iron deposits in any part of the system that is exposed to oxygen by aeration or mixing with water of a different quality. When pH and redox potential, Eh, are plotted on an iron stability diagram, additional information concerning the water's capacity to corrode or protect iron surfaces is obtained. If the geothermal water parameters plot in the ferrous ion area of the diagram, the water can be expected to dissolve iron. If they plot in the ferric hydroxide area, corrosion will be inhibited by oxidation products, and scaling may occur.

And finally a few words about **temperature**. An elevated temperature is most damaging to well water of high carbon dioxide content and low pH. The hydrogen evolution reaction rate doubles for each 10˚C increase in temperature. A water of 35˚C will, therefore, be twice as destructive to steel as one at 25˚C. At higher temperatures this effect can be extremely damaging.

Scale deposition can influence the corrosion of metals. Calcium carbonate scale is sometimes deposited intentionally in order to provide protection against corrosion. More often, however, scale deposits accelerate corrosion rates. Iron sulphide scale deposits cause particularly severe problems. The iron sulphide is cathodic to iron, setting up a galvanic cell subsequently causing severe pitting. The presence of any type of deposit in water containing gases (hydrogen sulphide, oxygen or carbon dioxide) will usually increase the severity of any potential corrosion problem.

Scaling or solid deposition is another aspect of geothermal fluid chemistry that influences material performance. Precipitation of solid phase species from a solution or on equipment surfaces can influence corrosion rates and cause erosion. The composition of the solids formed by scaling and the rate of precipitation depend on the fluid composition and specific process stream conditions; therefore, solids formed by scaling are not included in the list of key corrosion species.

Generally, the aggressiveness of a particular species varies from one material to the next. Often the interaction of two or more species with specific materials has a different effect from that of each species on its own. Also, the temperature dependence of the corrosion of a given material by a given species is often undefined. Finally, the importance of a given species depends on the form of attack under consideration.

5.3 Prediction of corrosion

As stated earlier the concentrations of chemical constituents in geothermal water can be used to predict the kinds of problems which might be encountered. Corrosion and scaling processes are complex and interactive. For this reason, no single test or index is an infallible indicator of these processes. Nevertheless, certain accelerated performance tests and indices already mentioned have proven to be of considerable value in selecting construction materials. If the geothermal water is saturated or supersaturated with respect to calcite, mineral scaling may occur along with moderate corrosion. Localized corrosion processes, such as that related to bacterial sulphate reduction, can cause severe damage to steel. The pH value can be used as a semiquantative indicator of the probable intensity or corrosion attack, as well as an indicator of the water's tendency to cause scaling rather than corrosion. Waters with pH below 6.5 are likely to be severely or extremely corrosive to steel and moderately corrosive to alloys such as brass (yellow and red). Waters with pH above 7.5 are more likely to be moderately or mildly corrosive to steel. Scaling may occur at a higher pH, particularly on steel surfaces.

A water saturated with calcium carbonate tends to precipitate a scale which may protect against corrosion. The degree of calcite saturation is a useful index in corrosion and scaling studies. Water of a high carbon dioxide concentration may be more destructive than conventional criteria indicate. There is reason to suspect significant localized damage at least to iron and steel when the carbon dioxide concentration exceeds 20 mg/l, regardless of the index value.

Redox potential-pH diagrams, which summarize the thermodynamic properties of a system, are extensively used for interpreting the corrosive behaviour of metals in geothermal water. Redox potentials are very useful in predicting corrosive behaviour. All metals with redox potentials more negative (active) than hydrogen will tend to be corroded by acid solutions. If dissolved oxygen is present, there is a possibility of oxygen reduction and corrosion. The application of thermodynamics to corrosion phenomena was generalized by M.Pourbaix with Eh/pH diagrams. The diagrams are constructed from calculations based on the Nernst equation and solubility data for various metal compounds (Hayashi,

1988). The relationship of oxidizing and reducing constituents determined by measuring the potential between a platinum and a reference electrode immersed in the water, can have a significant effect on the corrosiveness. This potential, which is called the redox potential or the Eh value, together with the corresponding pH value, indicates the ionic and molecular forms likely to be present in the particular water being tested, and thus, reveals whether metal dissolution or metal protection can be expected. For example, if the ferrous ion is the stable form, corrosion would be expected to proceed because this ion is soluble and a non-protective product of the anodic corrosion process. On the other hand, if semi-protective ferric hydroxide predominates, the water will be less aggressive to steel.

It is possible to delineate areas in which iron, iron-hydroxide, ferrous ions, etc., are thermodynamically stable. The Eh/pH diagrams represent equilibrium conditions and should never be used to predict the rate of a reaction. Although the spontaneous direction of a reaction may be in the direction of metal corrosion, this does not necessarily indicate that corrosion will take place. The rate of corrosion is another problem (Hayashi, 1988). In the analysis of corrosion phenomena, it is necessary to have some knowledge of the equilibrium conditions in the system. Such information not only indicates whether or not any given process is spontaneous, but also defines the conditions that must be achieved in order to minimize the effects of corrosion in practical systems.

6. APPLICATION OF SCALE PREDICTION MODELS TO KEBILI GEOTHERMAL FIELD

6.1 Analysis by X-ray diffraction

One scale sample and two samples from the asbestos cement pipeline, before and after the cooling tower of Kebili- Ras elaïn, were analyzed in the Orkustofnun laboratory in Iceland by using the X-ray diffraction machine (XRD). The photograph of the scale sample is shown in Figure 5.

In order to know the state of chemical composition of the elements in a sample, a fine grain sample is prepared. The evaluation consists of analysing the sample first by microscope, then after it had been put on the glass slide, a small quantity of acetone is added and the slide placed in the machine. The X-ray diffraction machine has a scale from 100 for the strongest line down to 10 or 5 for the weakest. The plane spacing (d), and intensity (I) corresponding to each line on the pattern are calculated (Cullity, 1978).

FIGURE 5: Photograph of Kebili scale sample

Each sample was identified from the diffraction pattern with the help of a computer program by locating in the file of known patterns one which exactly matched the pattern of the unknown, and then pattern-by-pattern comparison in order to find a match between the known and the unknown pattern.

The X-ray diffraction analysis gave the following results:

1. The scale sample from inside the pipeline after the cooling tower showed only the existence of aragonite ($CaCO_3$). The characteristic curve of this sample and the corresponding known pattern are shown in Figure 6 and one should notice the excellent match.

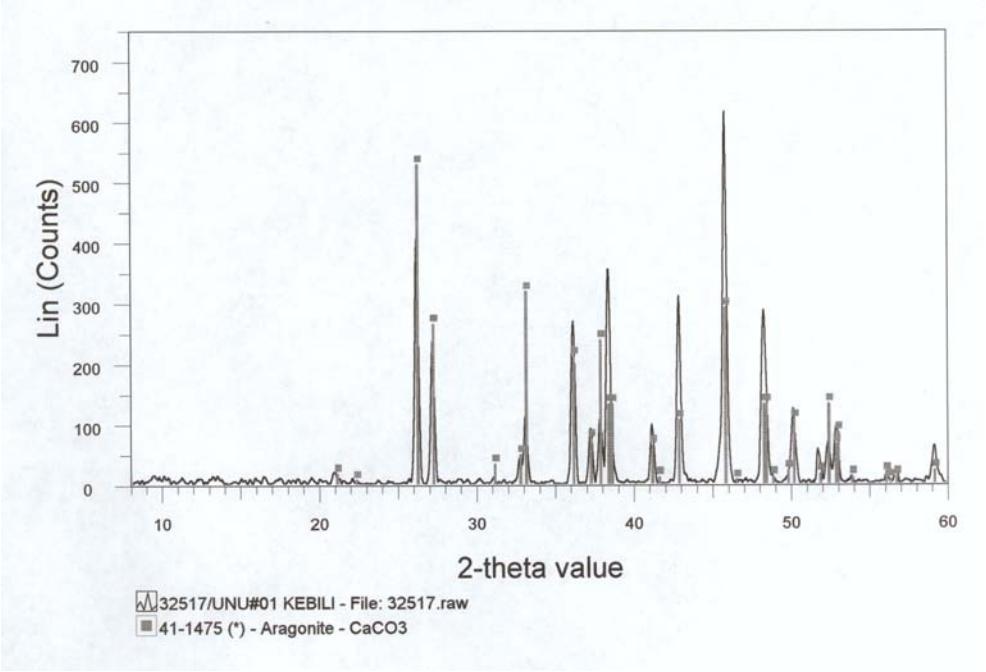

FIGURE 6: XRD analysis of scale sample from inside the Kebili-Ras Elaïn pipeline after the cooling tower

2. The two pipeline samples (samples of asbestos cement pipeline from before and after the cooling tower) showed the existence of aragonite ($CaCO_3$), calcite ($CaCO_3$), portlandite ($Ca(OH)_2$) and chrysotile ($3MgO.2SiO_2.2H_2O$). Figures 7 and 8 show the XRD analysis of the asbestos cement pipeline samples before and after the cooling tower, respectively.

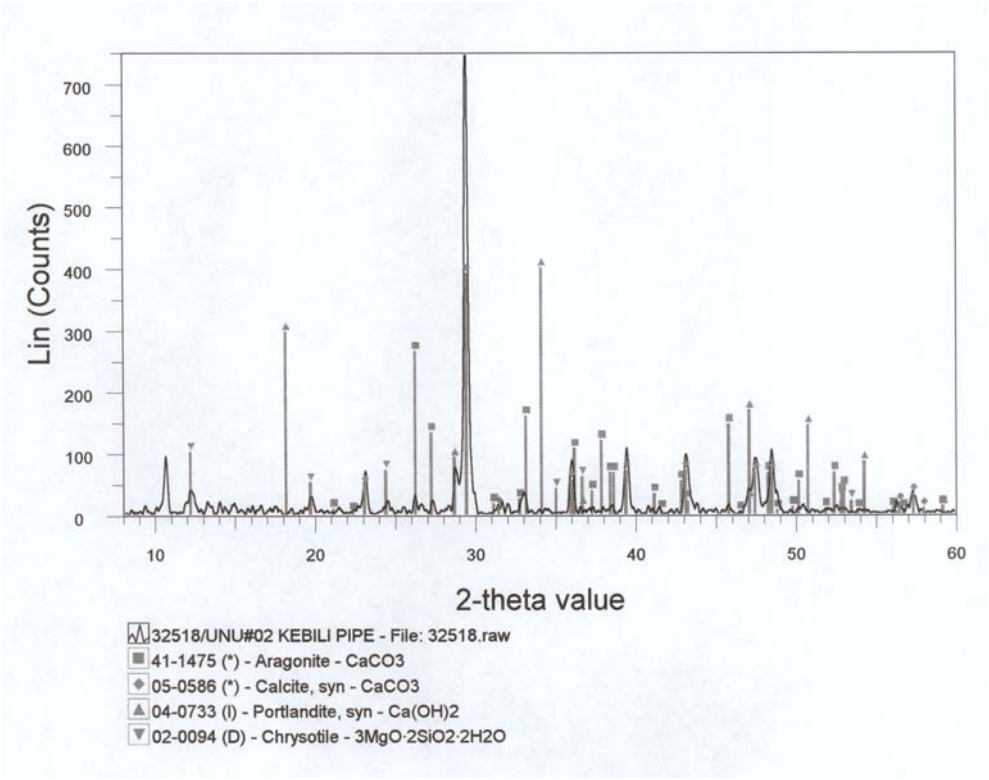

FIGURE 7: XRD analysis of the asbestos cement pipeline sample before the cooling tower

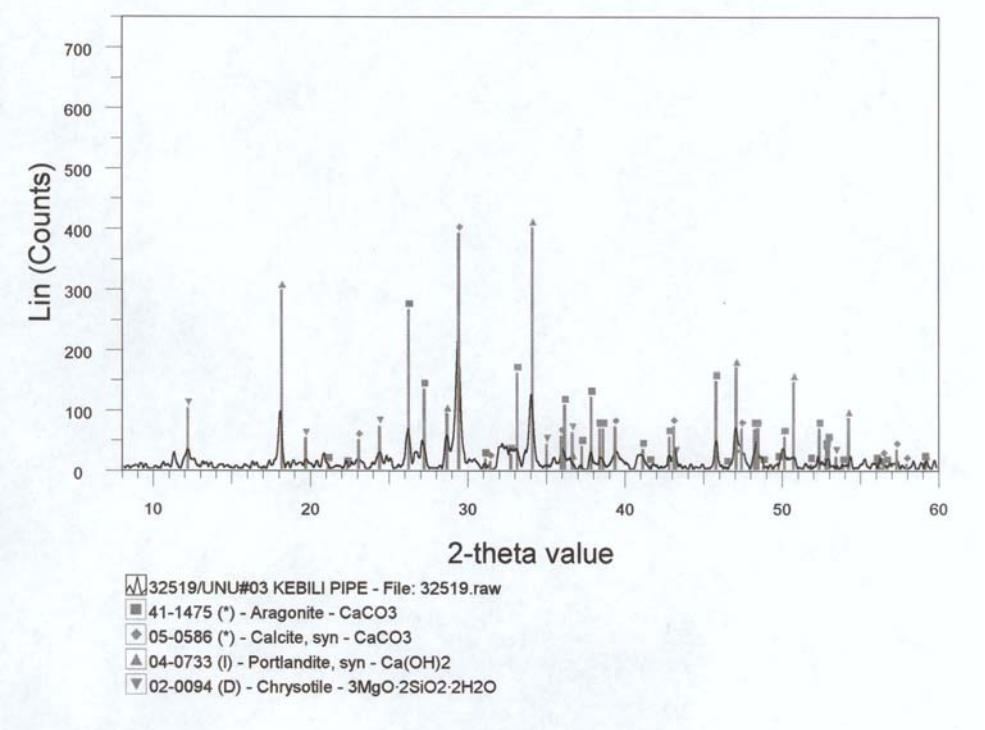

FIGURE 8: XRD analysis of the asbestos cement pipeline sample after the cooling tower

6.2 Geothermal water composition and mineral equilibria

Water chemistry data from three wells, Om Somaa-C.I.5, Lymagues-C.I.8, and Kebili-Ras Elaïn-C.I.10, in the Kebili geothermal field are used in this report for illustrative calculations of liquid composition and mineral equilibria (Table 3). The three wells are selected based on the carbonate dioxide content of their waters as representing the field. Well C.I.5 has the highest value, well C.I.8 has the lowest value, and well C.I.10 represents the middle value in the field and the scale sample was collected from it. Analytical data required and water sampling methods are given in Appendix I.

The geothermal water in Kebili undergoes three step changes during its flow from the well to the oasis area. From the well to the cooling tower, it is cooled in the pipeline about 2-3˚C. In the distributor basin at the top of the cooling tower, the water is cooled by aeration and degassing about 4-5˚C, where chemical reactions resulting from evaporation and degassing appear, especially the transfer of CO_2 from the liquid to the gas phase. Then, through the cooling tower, it is cooled by aeration, by maximising the water surface contact with air in order to obtain a final water temperature of 25-30˚C, suitable for oasis irrigation.

6.2.1 Kebili-Ras Elaïn-C.I.10

According to the data given in Tables 2 and 3, the temperature of the water is 66˚C, pH is 8.2 and the carbonate dioxide content is 145 mg/l. The chemical analysis was entered into the WATCH program for the study of calcite (see Appendix II) and the results were used to compute the saturation index (SI = log Q/K).

For calculating the saturation index of aragonite, two methods were used. The first step (conductive cooling between well and cooling tower), was computed by the SOLVEQ program. The rest, adiabatic

boiling, degassing and conductive cooling, by combining the theoretical value which was calculated by the formula given in Chapter 4.3 (Plummer and Busenberg, 1982), and the calculated value for the same temperatures, from the WATCH program, due to the equilibrium between calcite and aragonite (the two polymorphs have the same ionic activity). The results are listed in Table 6 and shown in Figure 9.

The water is highly supersaturated with respect to calcite and aragonite at wellhead temperature, and becomes more supersaturated within the cooling tower due to degassing of CO_2 (Reactions 8 and 9 in Chapter 4.3).

A loss of dissolved CO_2 to the gas phase leads to an increase in water pH. The result of pH calculations by the WATCH program are listed in Table 7, and Figure 10 shows the pH changes during the three steps of water cooling.

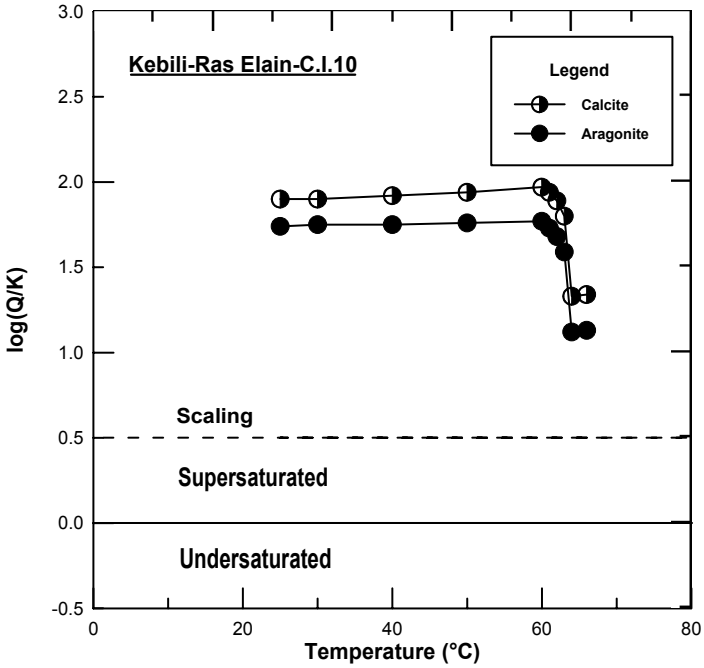

FIGURE 9: Calcite and aragonie saturation index during utilization of water from Ras-Elaïn C.I.10 (from initial data)

TABLE 6: Calcite and aragonite calculations for well Ras Elaïn-C.I.10.

Step	T (˚C)	Log Q (calculated)	Log K - calcite	log (Q/K) - calcite	log K - Aragonite	log (Q/K) - Aragonite
Wellhead	66	-7.579	-8.917	1.34	-8.705	1.13
Conductive cooling	64	-7.565	-8.890	1.33	-8.682	1.12
Degassing	63	-7.079	-8.877	1.80	-8.671	1.59
do.	62	-6.976	-8.864	1.89	-8.659	1.68
do.	61	-6.914	-8.852	1.94	-8.648	1.73
do.	60	-6.869	-8.839	1.97	-8.638	1.77
Conductive cooling	50	-6.778	-8.720	1.94	-8.536	1.76
do.	40	-6.697	-8.616	1.92	-8.446	1.75
do.	30	-6.625	-8.528	1.90	-8.370	1.75
do.	25	-6.592	-8.490	1.90	-8.336	1.74

TABLE 7: pH changes during the cooling of the water

Step	Temperature (˚C)	pH
Wellhead	66	7.83
Conductive cooling	64	7.85
Degassing	63	8.44
Degassing	62	8.58
Degassing	61	8.68
Degassing	60	8.75
Conductive cooling	50	8.86
Conductive cooling	40	8.98
Conductive cooling	30	9.11
Conductive cooling	25	9.18

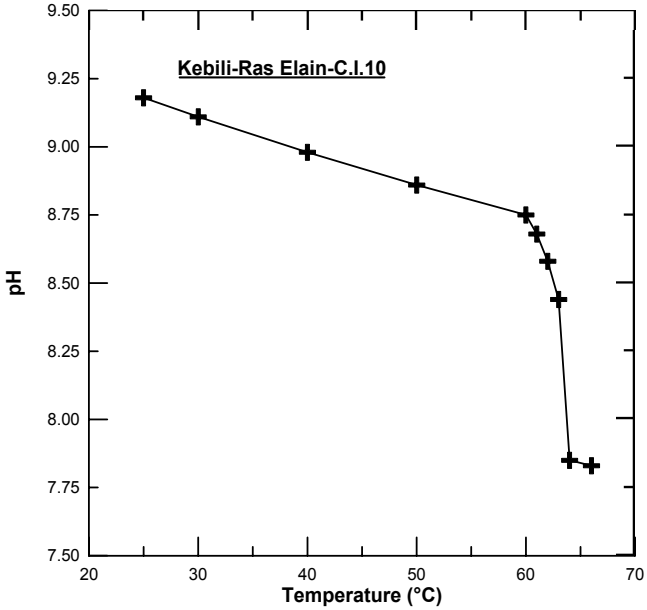

FIGURE 10: pH changes during the three steps of degassing and water cooling in the C.I.10 network

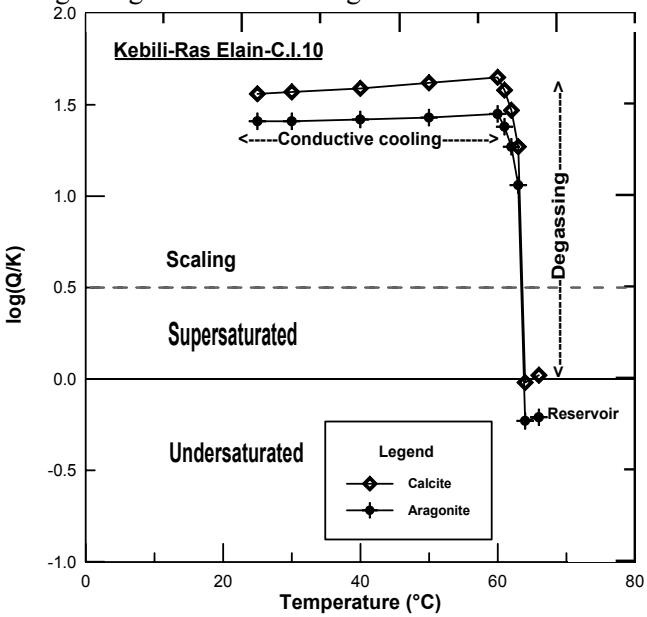

FIGURE 11: Saturation index of calcite and aragonite for Kebili-C.I.10

Studies of geothermal fluid chemistry in different parts of the world indicate that the water at depth in a geothermal reservoir is very close to being calcium carbonate saturated. Due to the possibility of a loss of CO_2 from the sample during transport from wellhead to laboratory, the assumption has been made in this study that the sample was saturated with respect to calcium carbonate in the reservoir. The CO_2 value of the sample has, therefore, been increased to 173 mg/l and the pH lowered to 6.5. It is also assumed that pH was measured at room temperature, 25˚C. Those changes will affect the degree of supersaturation of the water samples, but will not change the main result of this study.

After running the WATCH program for calcite calculations and the SOLVEQ for aragonite and combining the calculated value and theoretical value of solubility for aragonite, the results are listed in Table 8. Figure 11 shows the result and demonstrates an increase in the saturation index for the calcium carbonate polymorphs during water movement in the network.

The pH is affected drastically by the chemical changes of the water, due to the loss of dissolved gases, especially carbon dioxide. Figure 12 shows the increase of pH values from the wellhead to the bottom of the cooling tower.

TABLE 8: Saturation index calculations of aragonite for C.I.10

Temperature (˚C)	Log Q (calculated)	log K (theoretical)	SI log(Q/K)
66	-8.915	-8.705	-0.21
64	-8.914	-8.682	-0.23
63	-7.608	-8.671	1.06
62	-7.391	-8.659	1.27
61	-7.273	-8.648	1.38
60	-7.193	-8.638	1.45
50	-7.105	-8.536	1.43
40	-7.027	-8.446	1.42
30	-6.957	-8.37	1.41
25	-6.925	-8.336	1.41

6.2.2 Om Somaa-C.I.5

The well Om Somaa-C.I.5 is located 25 km northwest of Kebili-Ras Elaïn-C.I.10. The curves from the initial data are similar to the curves obtained from well Ras Elaïn-C.I.10.

In order to obtain equilibrium at the wellhead, the chemical data presented in Table 3 were changed with respect to pH and CO_2 and the following data were assumed: The temperature is 70.9˚C, the carbon dioxide value is increased from 211 to 252.5 mg/l and pH is lowered from 8.0 to 6.5.

The calcite calculation was computed with the WATCH program. In order to compute the aragonite calculations, the SOLVEQ program and the combination between the WATCH program and theoretical values of the carbonates solubility were used. Table 9 lists the results of calcite and aragonite calculations, and Figure 13 shows the curves corresponding to these results.

The pH changes through different parts of the network. The corresponding curve is shown in Figure 14.

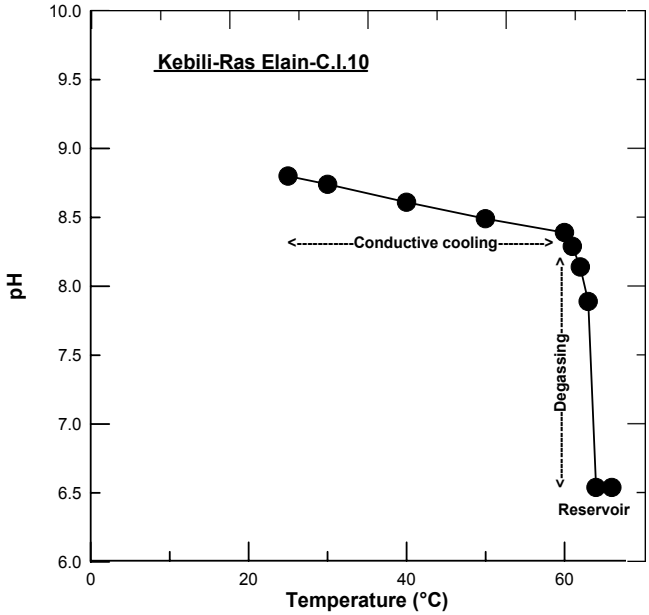

FIGURE 12: Increase of pH values in the Ras-Elaïn-C.I.10 system

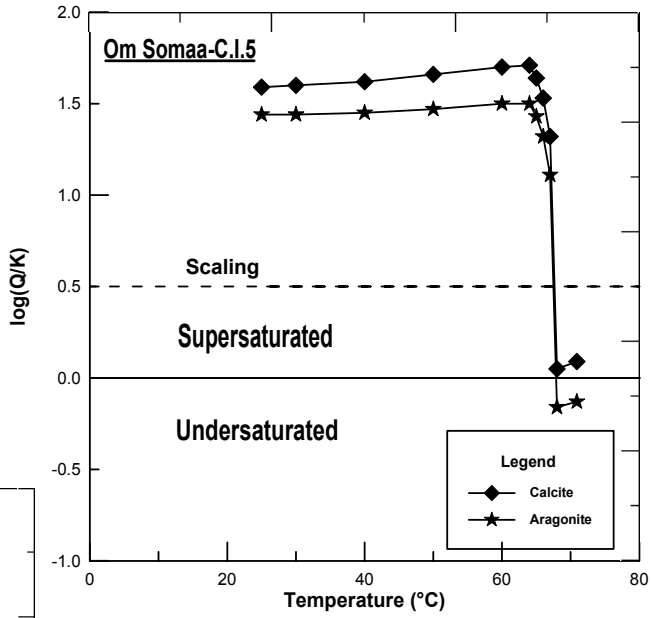

FIGURE 13: Saturation index, log (Q/K), for aragonite and calcite vs. temperature for the C.I.% network

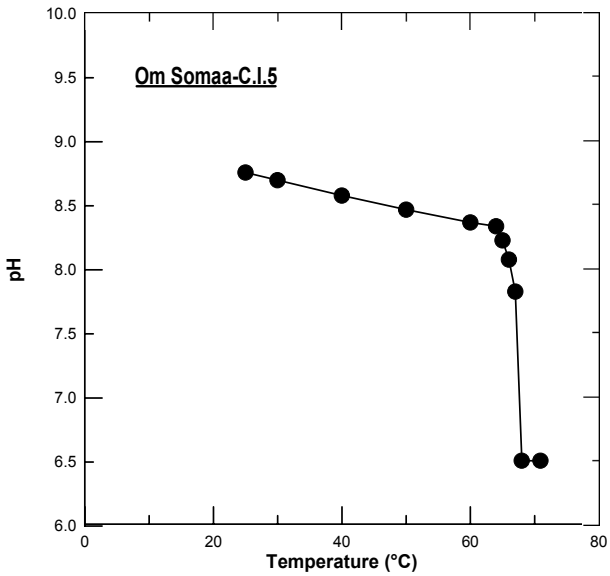

FIGURE 14: The change of pH in Om Somaa-C.I.5

TABLE 9: Aragonite and calcite calculations of Om Somaa-C.I.5 network

Temperature (˚C)	Log Q calculated	Log K (theo.) (aragonite)	log (Q/K) (aragonite)	log K (theo.) (calcite)	Log (Q/K) (calcite)
70.9	-8.892	-8.763	-0.13	-8.984	0.09
68	-8.892	-8.728	-0.16	-8.944	0.05
67	-7.61	-8.716	1.11	-8.930	1.32
66	-7.385	-8.705	1.32	-8.917	1.53
65	-7.262	-8.693	1.43	-8.904	1.64
64	-7.178	-8.682	1.50	-8.890	1.71
60	-7.143	-8.638	1.50	-8.839	1.70
50	-7.064	-8.536	1.47	-8.720	1.66
40	-6.992	-8.446	1.45	-8.616	1.62
30	-6.929	-8.37	1.44	-8.528	1.60
25	-6.90	-8.336	1.44	-8.490	1.59

6.2.3 Lymagues-C.I.8

Geothermal well-C.I.8 is located 15 km east of Kebili-C.I.10. Based on the initial data, the water from well C.I.8 is highly supersaturated at wellhead with respect to the calcium carbonate minerals, and becomes increasingly more supersaturated as the water moves through the Lymagues network. As for the previous locations, the assumption has been made that during sampling and transport, CO_2 might have been lost and the pH, therefore, changed. Therefore, it is assumed that the water is in equilibrium with calcium carbonates at wellhead, and the CO_2 content has been increased from 62 to 124 mg/l and the pH lowered from 8.3 to 6.6 for the present calculations.

The results of calcite and aragonite calculations, using the WATCH and SOLVEQ programs with the theoretical calculations, are listed in Table 10 and shown in Figure 15.

The different values of the water pH corresponding to each temperature step are shown in Figure 16 which explains the increase of water pH from the wellhead to the supply pipeline.

TABLE 10: Saturation index calculations of calcite and aragonite for Lymagues-C.I.8

Temp. (˚C)	log Q calculated	Log K (theo.) (aragonite)	log (Q/K) (aragonite)	log K (theo.) (calcite)	log (Q/K) (calcite)
72.5	-9.005	-8.782	-0.22	-9.006	0.001
70	-9.003	-8.752	-0.25	-8.971	-0.03
69	-7.780	-8.740	0.96	-8.958	1.18
68	-7.571	-8.728	1.16	-8.944	1.37
67	-7.457	-8.716	1.26	-8.930	1.47
66	-7.379	-8.705	1.33	-8.917	1.54
65	-7.320	-8.693	1.37	-8.904	1.58
60	-7.271	-8.638	1.37	-8.839	1.57
50	-7.181	-8.536	1.36	-8.720	1.54
40	-7.101	-8.446	1.35	-8.616	1.52
30	-7.030	-8.370	1.34	-8.528	1.50
25	-6.999	-8.336	1.34	-8.490	1.49

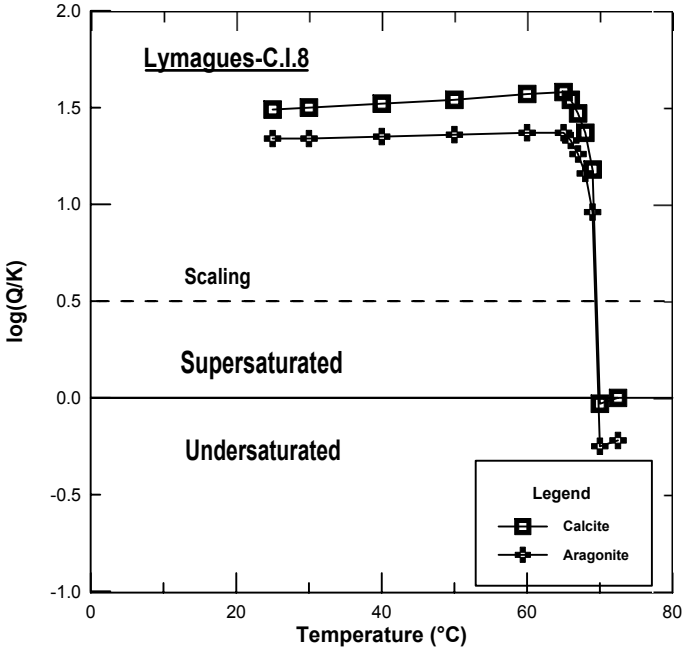

FIGURE 15: Saturation index of calcite and aragonite for Lymagues-C.I.8

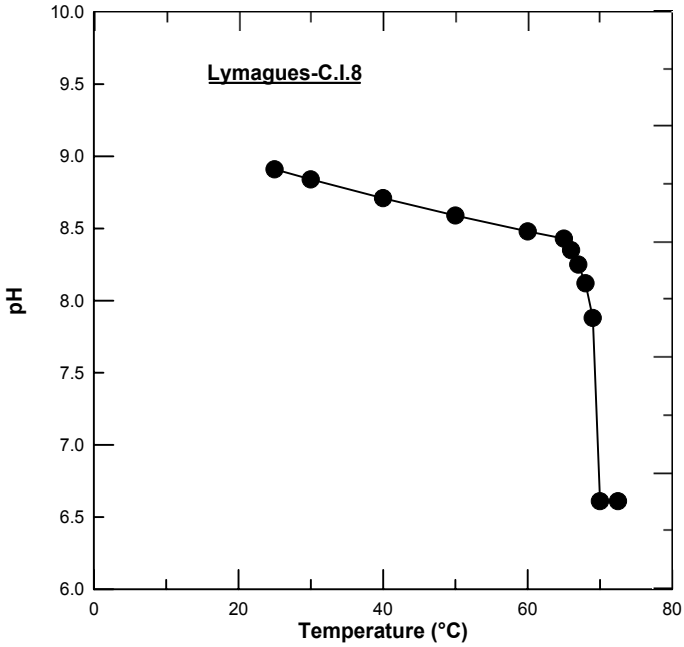

FIGURE 16: pH increase against temperature for the C.I.8 network

7. DISCUSSION

Two chemical models were used to analyse calcium carbonate (calcite and aragonite) scaling potential in the water from the low-temperature geothermal field in Kebili. The supply pipeline becomes plugged due to mineral deposition (aragonite) after degassing and cooling in a cooling tower.

The WATCH program is a good way to study solution and calcite equilibria, as well as the SOLVEQ program for the study of aragonite equilibria, especially chemical changes in water chemistry accompanying variable degassing and cooling, and how these changes affect the calcite and aragonite equilibria.

Three steps of chemical changes occur: Conductive cooling in the pipeline from the well to the cooling tower, adiabatic boiling (degassing by evaporation) in the inlet basin of the cooling tower, and conductive cooling through the cooling tower. In order to study the aragonite equilibria, a combination of calculations based on the SOLVEQ program, WATCH program and theoretical reactions were used.

A scale sample from inside the supply pipeline was analysed by an XRD machine, giving information about its origin as aragonite.

Complete data are very important for any calculation and analysis. In this report, data from three selected wells were used representing the entire field, according to their different carbon dioxide values. Starting from saturated conditions, the saturation index and pH curves for the three selected waters show an increase of log (Q/K) for both calcite and aragonite, as well as an increase of pH values during the three steps. As mentioned in Chapter 4.3, calcium carbonate precipitates can form in geothermal waters by combining calcium ions and carbonate ions. The calcite scales form very rapidly once the thermodynamic conditions are suitable. The loss of carbon dioxide (by degassing in the cooling tower) and the associated pH increase are the principal causes for calcium carbonate precipitation.

Results from this study show that the water entering the supply pipeline is highly supersaturated with aragonite and calcite. The final saturation index values of calcite and aragonite as the water enters the supply pipeline for the three selected well data are listed in Table 11 and shown in Figure 17.

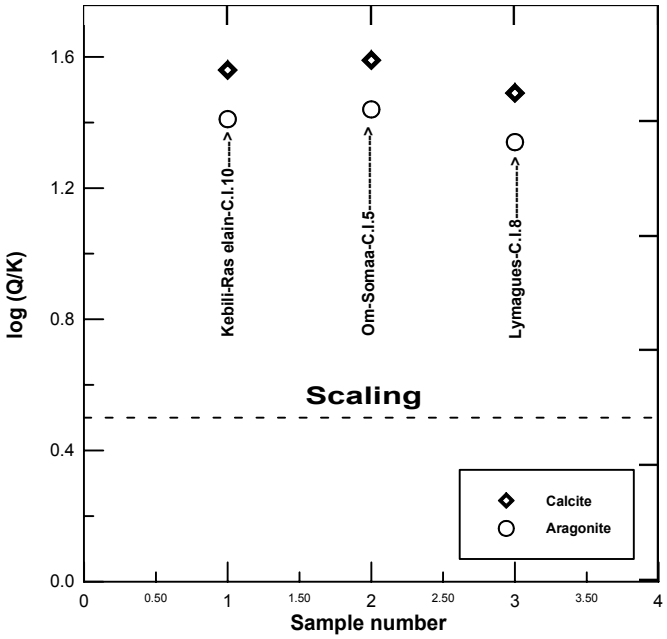

FIGURE 17: Log (Q/K) for aragonite and calcite in final step in the three selected network pipelines

TABLE 11: The saturation index, log (Q/K), for aragonite and calcite in the final steps for the three selected wells in Kebili

Site	log (Q/K) (calcite)	log (Q/K) (aragonite)
Kebili-C.I.10	1.56	1.41
Om-Somaa-C.I.5	1.59	1.44
Lymagues-C.I.8	1.49	1.34

According to Icelandic experiences in studies of scaling problems in geothermal fields, we can determine the criterion for the formation of calcite and aragonite scaling. The saturation index boundary between calcium carbonate scaling and no scaling in some geothermal fields in Iceland are listed in Table 12.

TABLE 12: The saturation index boundary between calcite scaling and no scaling in Iceland (Bai Liping, 1991)

Geothermal field	Saturation index boundary (SI)
Hrísey	0.36-0.5
Laugarnes	0.43-0.48
Sudureyri	0.37-0.48
Selfoss	< 0.28 (except ThK-11)
Boundaries	0.36-0.5

Empirically it has been shown that no deposits are found even though the water becomes supersaturated if the saturation index does not go above 0.5. Figure 18 shows the relationship between the degree of calcite supersaturation and calcite scaling in selected wells in Iceland.

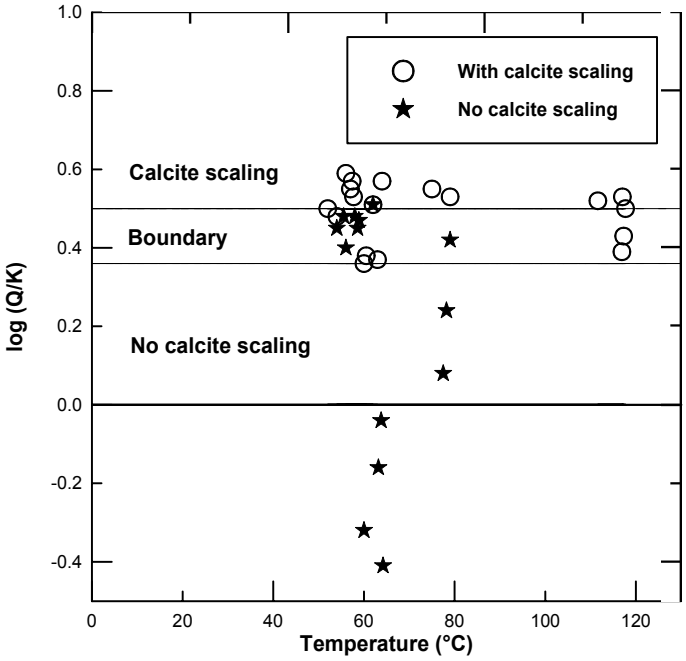

FIGURE 18: $CaCO_3$ supersaturation in selected wells in Iceland

These results indicate that if the saturation index, log (Q/K), is higher than 0.5, a calcite scaling problem occurs; if the calcite saturation index is lower than 0.36, there is no calcite scaling, and between 0.36 and 0.5, calcite scaling may and may not occur, depending on the flow turbulence, chemical composition (salinity) corrosion, etc. This implies a calcite supersaturation ratio (Q/K) of 2.3-3.2.

The ratio (Q/K) of 22 to 39 obtained for the Tunisian waters will result in rapid scaling inside the supply pipeline, but a saturation index for water in the repression pipeline from well to the cooling tower shows that it will be clean.

8. CONCLUSIONS

Scaling sample and pipeline samples from the Kebili- Ras Elaïn network were identified by X-Ray Diffraction. It was confirmed that the scale deposit inside the supply pipeline is aragonite ($CaCO_3$).

Chemical composition of water from three wells; Kebili- C.I.10, Om Somaa- C.I.5 and Lymagues- C.I.8 were analysed by using the WATCH and the SOLVEQ geochemical programs, which give information about the mineral equilibria and a basis to assess possible scaling problems. The study shows:

- An increase of pH through the network due to the degassing in the top of the cooling tower;
- The water becoming highly supersaturated with respect to aragonite and calcite;
- There is only scaling after going through the cooling tower and not in the repression pipeline from the well to the cooling tower, due to the effect of the degassing that causes calcium carbonate deposition;
- The saturation index SI= log Q/logK reaches a value of 1.3-1.5, but experience has shown that rapid scaling occurs when SI > 0.5.

For monitoring of scaling and corrosion, corrosion coupons (Appendix III) should be installed in many sites of the network, such as in the wellhead, in the basin of the cooling tower and in the supply pipeline.

It is better to counteract scaling and corrosion problems before they occur. For monitoring of the field (reservoir and surface equipment) and possible scaling and corrosion, it is recommended to take samples for complete analysis twice a year, and weekly samples for selected components.

To mitigate the problems caused by calcite and aragonite deposition in geothermal water in Kebili, the following actions should be considered:

- To replace the asbestos cement pipes where the topography allows by building open canals (canal semi circulaire and seguias betonnées) in order to facilitate maintenance and contribute to cooling of the water before use;
- To use holding ponds to allow scales to form and for the water to be reequilibrated before entering the pipeline;
- To use plastic pipe instead of the asbestos cement pipeline for reduced roughness. The asbestos cement contains some calcium carbonate and can accelerate deposition;
- To use inhibitors in order to reduce the amount or rate of scale formation and/or rendering the scale easier to remove during periodic cleaning operations. These inhibitors need to be acceptable for plants.

ACKNOWLEDGEMENTS

I admire my advisor Sverrir Thórhallsson, who is scrupulous and serious in his work, and I would like to express my gratitude to him for his unselfish devotion and excellent guidance and supervision during the whole period and for formulating the final report and critically evaluating it. Special thanks to Dr. Ingvar Birgir Fridleifsson, the director of the UNU Geothermal Training Program for his selection of candidates for the course and making elaborate arrangements. Lúdvík S. Georgsson, the deputy director, and Ms. Gudrún Bjarnadóttir are thanked for their assistance and useful advice during the whole course. Thanks to Magnús Ólafsson for his suggestions for my project and for his directions on how to run the WATCH and SOLVEQ programs, to Sigurdur Sveinn Jónsson for his help in the analytical work; to all the people who gave me help at Orkustofnun.

I also wish to thank Mr. Saad Seddik and Mohamed Ghrissi, respectively the regional commissar for agricultural development of Kebili and head of the rural engineering department for giving me the opportunity to undertake this training, as well as my parents and my wife Kalthoum for encouraging me to participate in this course.

REFERENCES

Arnórsson, S., 1978: Precipitation of calcite from flashed geothermal waters in Iceland. *Contrib. Mineral. Petrol. 66,* 21-28.

Arnórsson, S., Sigurdsson, S. and Svavarsson, H., 1982: The chemistry of geothermal waters in Iceland I. Calculation of aqueous speciation from 0˚C to 370˚C. *Geochim. Cosmochim. Acta, 46,* 1513-1532.

Arnórsson, S., 1989: Deposition of calcium carbonate minerals from geothermal waters-theoretical considerations. *Geothermics, 18,* 33-39.

Bai Liping, 1991: *Chemical modelling programs for predicting calcite scaling, applied to low-temperature geothermal waters in Iceland*. UNU G.T.P., Iceland, report 3, 45 pp.

Ben Dhia, H., and Bouri, S., 1995: *Overview of geothermal activities in Tunisia*. Ecole Nationale d'Ingenieurs de Sfax, Tunisia, 5 pp.

Ben Mohamed, M., 1997: Agricultural geothermal utilization in Kébili region, Tunisia. Report 2 in: *Geothermal Training in Iceland1997.* UNU G.T.P., Iceland, 27-56.

Bjarnason, J.Ö., 1994: *The speciation program WATCH, version 2.1.* Orkustofnun, Reykjavík, 7 pp.

Cowan, J.C., and Weintritt, D.J., 1976: *Water-formed scale deposits.* Gulf Publishing Co., Houston, TX, 596 pp.

CRDA, 1996: *Annual reports 1996*. CRDA, Kébili, Tunisia, regional report (in French), 113 pp.

Criaud, A., and Fouillac, C., 1989: Sulfide scaling in low-enthalpy geothermal environments. A survey. *Geothermics, 18,* 73-81.

Cullity, B.D., 1978: Chemical analysis by X-ray diffraction. *Elements of X-Ray Diffraction, 2nd edition,* 397-420.

Ellis, A. J., 1959: The solubility of calcite in carbon dioxide solutions. *Am. J. Sci., 257,* 354-365.

Hayashi, Y., 1988: *Fundamentals of corrosion.* No. 29 textbook of the IGTCGE, Kyushu, Japan.

Honegger, J., Czernochowski-Lauriol, I., Criaud, A., Menjoz, A., Sainson, S., and Gvezennec, J., 1989: Detailed study of sulfide scaling at La Courenve-Nord, a geothermal exploitation of the Paris Basin, France. *Geothermics, 18,* 137-144.

Janik, C., 1985: *Chemical data collection and geochemical applications in reservoir engineering.* Geoth. Resources Council, Course on engineering and economic assessment of geothermal resources, August 1985, Hawaii.

Kindle, C.H., Mercer, B.W., Elmore, R.P., Blair, S.C., and Myers, D.A., 1984: *Geothermal injection treatment: Process chemistry, field experience and design options.* Battelle Pacific Northwest Laboratories, Richland, WA, report PNL-4767 / UC-66d.

Kristmannsdóttir, H., 1989: Types of scaling occurring by geothermal utilization in Iceland. *Geothermics, 18,* 183-190.

Mamou, A., 1992: *Notes on geothermal resources utilized in Tunisia.* Direction Generale des Ressouces en Eaux, Tunisia, ministerial report (in French), 24 pp.

Miller, P., 1952: A portion of the system calcium carbonate - carbon dioxide - water with geological implications. *Am. J. Sci., 250,* 161-203.

Plummer, L.N., and Busenberg, E., 1982: The solubilities of calcite, aragonite and vaterite in CO_2-H_2O solutions between 0 and 90˚C, and an evaluation of the aqueous model for the system $CaCO_3$-CO_2-H_2O. *Geochim. Cosmochim. Acta, 46,* 1011-1040.

Reed, M.H., and Spycher, N.F., 1984: Calculation of pH and mineral equilibria in hydrothermal water with application to geothermometry and studies of boiling and dilution. *Geochim. Cosmochim. Acta, 48*, 1479-1490.

Said, M., 1997: Geothermal utilisation for heating, irrigation and soil disinfection in greenhouses in Tunisia. Report 13 in: *Geothermal Training in Iceland 1997*. UNU G.T.P., Iceland, 311-338.

Sharp, W., and Kennedy, G., 1965: The system CaO-CO_2-water in the two-phase region calcite and aqueous solution. *J. Geol., 73,* 391- 403.

Spycher, N.F., and Reed, M.H., 1989: *User´s guide for SOLVEQ: A computer program for computing aqueous-minerals-gas equilibria (revised prelim. edition)*. University of Oregon, Eugene, OR, 37 pp.

Stanasel, O., 1996: *Assessment of production characteristics of geothermal fluids and monitoring of corrosion and scaling at Oradea, Romania and Seltjarnarnes, Iceland.* Report 16 in: *Geothermal Training in Iceland 1996*. UNU G.T.P., Iceland, 363-398.

Stefánsson, V., 1986: *Report on an advisory mission 1986 in Tunisia*. United Nations, New York, report, 24 pp.

Thomas, D., and Gudmundsson, J., 1989: Advances in the study of solids deposition in geothermal systems. *Geothermics, 18,* 5-15.

Ungemach, P., and Roque, C., 1988: Corrosion and scaling of geothermal wells in the Paris basin. Damage diagnosis, removal and inhibition. *Proceedings of the International Workshop on Deposition of Solids in Geothermal Systems, Reykjavik, Iceland,* 31 pp.

Vuataz, F., Czernochowski-Lauriol, I., Fouillac, C., and Detoc, S., 1989: Chemical study of a low-temperature geothermal fluid in a Triassic sandstone aquifer: Scaling potential and fluid treatment. *Geothermics,18,* 313-320.

APPENDIX I: Analytical data and sampling methods

Analytical data required for thermodynamic modelling (liquid phase)

- Sampling pressure (bar)
- Source temperature (˚C)
- Enthalpy of liquid (MJ/Kg)
- pH/˚C liquid phase
- SiO_2 liquid phase (mg/kg)
- Na " " "
- Ca " " "
- Mg " " "
- CO_2 " " "
- SO_4 " " "
- H_2S " " "
- Cl " " "
- F " " "
- Al " " "
- Fe " " "
- B " " "
- NH_3 " " "

For sampling from low-temperature wells, the following equipment are used:

- Plastic bottles, 500 ml, four per sample;
- Plastic bottles, 100 ml, three to four per sample;
- Air tight glass bulbs, one per sample;
- Filter and filter paper (the size of the pores is 0.45 μm);
- Finnpipets and clean tips;
- One 100 ml and two 50 ml volumetric flasks for dilution (if SiO_2 expected > 100 ppm);
- Equipment for measuring dissolved oxygen;
- Cooling coil;
- Rubber hoses and plastic connections;
- Rubber gloves, water-resistant clothes and rubber boots;
- Fittings;
- Permanent marker;
- Field record card and pencil;
- Thermometer;
- Map showing the location of the well;
- Previous analysis of water if available;
- Distilled water;
- Solutions: HCl 6 N, HNO_3 suprapure, $Zn(CH_3COO)_2$ 0.2M if H_2S expected > 0.5 ppm..

For titration of H_2S (in situ) the following are also needed:

- Volumetric flasks, 50 ml, two;
- Erlenmeyer flasks, 100 ml, two;
- Gilmont Micrometer Buret;
- Finnpipet, preset at 5 ml;
- NaOH, solution 5N;
- Acetone;
- Dithizone powder as indicator;
- $Hg(CH_3COO)_2$, solution 0.001N;
- Tissues.

APPENDIX II: WATCH calculations for water sample from Kebili field

ICELANDIC WATER CHEMISTRY GROUP Program WATCH, version 2.1 / 1994

Elguedri/1999 analysis

kebili-Ras Elain-C.I.10

Water sample (mg/kg) Steam sample

pH/deg.C	6.64/ 25.0	Gas (volume %)		Reference temperature	deg.C : 66.0 (Measured)
CO2	173.11	CO2	.00		
H2S	.00	H2S	.00	Sampling pressure	bar abs. : 1.0
NH3	.00	NH3	.00	Discharge enthalpy	kJ/kg : 276.(Calculated)
B	.00	H2	.00	Discharge	kg/s : .0
SiO2	.00	O2	.00	Steam fraction at collection	: .0000
Na	402.32	CH4	.00		
K	41.05	N2	.00	Measured temperature	deg.C : 66.0
Mg	85.12				
Ca	248.50	Liters gas per kg			
F	.00	condensate/deg.C	.00/.0	Condensate (mg/kg)	
Cl	616.95			pH/deg.C	.00/ .0
SO4	745.43	Total steam (mg/kg)		CO2	.00
Al	.00	CO2	.00	H2S	.00
Fe	.00	H2S	.00	NH3	.00
TDS	2410.00	NH3	.00	Na	.00

Ionic strength = .04783

Ionic balance : Cations (mol.eq.) = .03473205 Anions (mol.eq.) = .03243903 Difference (%) = 6.83
Deep water pH is 6.543

log solubility products of minerals in deep water

	Theor.	Calc.		Theor.	Calc.		Theor.	Calc.
Adularia	-18.770	99.999	Albite, low	-17.899	99.999	Analcime	-14.263	99.999
Anhydrite	-5.155	-5.263	Calcite	-8.917	-8.915	Chalcedony	-3.136	99.999
Mg-Chlorite	-81.773	99.999	Fluorite	-10.641	99.999	Goethite	-5.885	99.999
Laumontite	-29.088	99.999	Microcline	-20.411	99.999	Magnetite	-32.297	99.999
Ca-Montmor.	-95.532	99.999	K-Montmor.	-47.035	99.999	Mg-Montmor.	-96.491	99.999
Na-Montmor.	-46.917	99.999	Muscovite	-23.578	99.999	Prehnite	-38.283	99.999
Pyrrhotite	-116.863	99.999	Pyrite	-172.699	99.999	Quartz	-3.449	99.999
Wairakite	-25.827	99.999	Wollastonite	11.976	99.999	Zoisite	-37.090	99.999
Epidote	-46.378	99.999	Marcasite	-146.941	99.999	Talc	18.018	99.999
Chrysotile	26.762	99.999	Sil. amorph.	-2.414	99.999			

First step Aquifer liquid cooled to 64.0 øC

Deep water pH is 6.544

log solubility products of minerals in deep water

	Theor.	Calc.		Theor.	Calc.		Theor.	Calc.
Adularia	-18.876	99.999	Albite, low	-17.995	99.999	Analcime	-14.336	99.999
Anhydrite	-5.130	-5.256	Calcite	-8.890	-8.914	Chalcedony	-3.156	99.999
Mg-Chlorite	-81.897	99.999	Fluorite	-10.651	99.999	Goethite	-5.953	99.999
Laumontite	-29.220	99.999	Microcline	-20.534	99.999	Magnetite	-32.451	99.999
Ca-Montmor.	-96.224	99.999	K-Montmor.	-47.408	99.999	Mg-Montmor.	-97.171	99.999
Na-Montmor.	-47.280	99.999	Muscovite	-23.747	99.999	Prehnite	-38.396	99.999
Pyrrhotite	-117.876	99.999	Pyrite	-174.276	99.999	Quartz	-3.472	99.999
Wairakite	-25.909	99.999	Wollastonite	12.051	99.999	Zoisite	-37.185	99.999
Epidote	-46.544	99.999	Marcasite	-148.367	99.999	Talc	18.175	99.999
Chrysotile	26.967	99.999	Sil. amorph.	-2.427	99.999			

Second step Aquifer liquid boiled to 63.0 øC Degassing coefficient is 1.0000

Deep water pH is 7.894

log solubility products of minerals in deep water

	Theor.	Calc.		Theor.	Calc.		Theor.	Calc.
Adularia	-18.929	99.999	Albite, low	-18.044	99.999	Analcime	-14.373	99.999
Anhydrite	-5.118	-5.254	Calcite	-8.877	-7.608	Chalcedony	-3.165	99.999
Mg-Chlorite	-81.960	99.999	Fluorite	-10.656	99.999	Goethite	-5.988	99.999
Laumontite	-29.287	99.999	Microcline	-20.596	99.999	Magnetite	-32.529	99.999
Ca-Montmor.	-96.575	99.999	K-Montmor.	-47.596	99.999	Mg-Montmor.	-97.514	99.999
Na-Montmor.	-47.464	99.999	Muscovite	-23.832	99.999	Prehnite	-38.454	99.999
Pyrrhotite	-118.384	99.999	Pyrite	-175.068	99.999	Quartz	-3.483	99.999
Wairakite	-25.950	99.999	Wollastonite	12.089	99.999	Zoisite	-37.233	99.999
Epidote	-46.628	99.999	Marcasite	-149.082	99.999	Talc	18.254	99.999
Chrysotile	27.071	99.999	Sil. amorph.	-2.433	99.999			

Second step Aquifer liquid boiled to 62.0 øC Degassing coefficient is 1.0000

Deep water pH is 8.143

log solubility products of minerals in deep water

	Theor.	Calc.		Theor.	Calc.		Theor.	Calc.
Adularia	-18.983	99.999	Albite, low	-18.093	99.999	Analcime	-14.410	99.999
Anhydrite	-5.106	-5.252	Calcite	-8.864	-7.391	Chalcedony	-3.175	99.999
Mg-Chlorite	-82.025	99.999	Fluorite	-10.662	99.999	Goethite	-6.022	99.999
Laumontite	-29.355	99.999	Microcline	-20.658	99.999	Magnetite	-32.607	99.999
Ca-Montmor.	-96.928	99.999	K-Montmor.	-47.786	99.999	Mg-Montmor.	-97.861	99.999
Na-Montmor.	-47.649	99.999	Muscovite	-23.918	99.999	Prehnite	-38.512	99.999
Pyrrhotite	-118.892	99.999	Pyrite	-175.862	99.999	Quartz	-3.494	99.999
Wairakite	-25.993	99.999	Wollastonite	12.127	99.999	Zoisite	-37.282	99.999
Epidote	-46.711	99.999	Marcasite	-149.800	99.999	Talc	18.334	99.999
Chrysotile	27.175	99.999	Sil. amorph.	-2.440	99.999			

Second step Aquifer liquid boiled to 61.0 øC Degassing coefficient is 1.0000

Deep water pH is 8.287

log solubility products of minerals in deep water

	Theor.	Calc.		Theor.	Calc.		Theor.	Calc.
Adularia	-19.038	99.999	Albite, low	-18.143	99.999	Analcime	-14.448	99.999
Anhydrite	-5.094	-5.249	Calcite	-8.852	-7.273	Chalcedony	-3.185	99.999
Mg-Chlorite	-82.090	99.999	Fluorite	-10.667	99.999	Goethite	-6.056	99.999
Laumontite	-29.423	99.999	Microcline	-20.721	99.999	Magnetite	-32.685	99.999
Ca-Montmor.	-97.284	99.999	K-Montmor.	-47.977	99.999	Mg-Montmor.	-98.210	99.999
Na-Montmor.	-47.835	99.999	Muscovite	-24.005	99.999	Prehnite	-38.571	99.999
Pyrrhotite	-119.400	99.999	Pyrite	-176.659	99.999	Quartz	-3.505	99.999
Wairakite	-26.035	99.999	Wollastonite	12.165	99.999	Zoisite	-37.332	99.999
Epidote	-46.795	99.999	Marcasite	-150.519	99.999	Talc	18.414	99.999
Chrysotile	27.280	99.999	Sil. amorph.	-2.446	99.999			

Second step Aquifer liquid boiled to 60.0 øC Degassing coefficient is 1.0000

Deep water pH is 8.388

log solubility products of minerals in deep water

	Theor.	Calc.		Theor.	Calc.		Theor.	Calc.
Adularia	-19.092	99.999	Albite, low	-18.193	99.999	Analcime	-14.486	99.999
Anhydrite	-5.082	-5.246	Calcite	-8.839	-7.193	Chalcedony	-3.195	99.999
Mg-Chlorite	-82.157	99.999	Fluorite	-10.673	99.999	Goethite	-6.090	99.999
Laumontite	-29.492	99.999	Microcline	-20.784	99.999	Magnetite	-32.763	99.999
Ca-Montmor.	-97.642	99.999	K-Montmor.	-48.170	99.999	Mg-Montmor.	-98.562	99.999
Na-Montmor.	-48.023	99.999	Muscovite	-24.092	99.999	Prehnite	-38.631	99.999
Pyrrhotite	-119.909	99.999	Pyrite	-177.458	99.999	Quartz	-3.517	99.999
Wairakite	-26.078	99.999	Wollastonite	12.204	99.999	Zoisite	-37.383	99.999
Epidote	-46.879	99.999	Marcasite	-151.241	99.999	Talc	18.494	99.999
Chrysotile	27.386	99.999	Sil. amorph.	-2.453	99.999			

Third step Aquifer liquid cooled to 50.0 øC

Deep water pH is 8.494

log solubility products of minerals in deep water

	Theor.	Calc.		Theor.	Calc.		Theor.	Calc.
Adularia	-19.664	99.999	Albite, low	-18.715	99.999	Analcime	-14.883	99.999
Anhydrite	-4.966	-5.213	Calcite	-8.720	-7.105	Chalcedony	-3.297	99.999
Mg-Chlorite	-82.885	99.999	Fluorite	-10.737	99.999	Goethite	-6.429	99.999
Laumontite	-30.213	99.999	Microcline	-21.446	99.999	Magnetite	-33.553	99.999
Ca-Montmor.	-101.365	99.999	K-Montmor.	-50.170	99.999	Mg-Montmor.	-102.214	99.999
Na-Montmor.	-49.974	99.999	Muscovite	-25.002	99.999	Prehnite	-39.270	99.999
Pyrrhotite	-125.035	99.999	Pyrite	-185.595	99.999	Quartz	-3.632	99.999
Wairakite	-26.535	99.999	Wollastonite	12.603	99.999	Zoisite	-37.927	99.999
Epidote	-47.739	99.999	Marcasite	-158.572	99.999	Talc	19.326	99.999
Chrysotile	28.483	99.999	Sil. amorph.	-2.521	99.999			

Third step Aquifer liquid cooled to 40.0 øC

Deep water pH is 8.610

log solubility products of minerals in deep water

	Theor.	Calc.		Theor.	Calc.		Theor.	Calc.
Adularia	-20.282	99.999	Albite, low	-19.280	99.999	Analcime	-15.313	99.999
Anhydrite	-4.857	-5.183	Calcite	-8.616	-7.027	Chalcedony	-3.406	99.999
Mg-Chlorite	-83.730	99.999	Fluorite	-10.816	99.999	Goethite	-6.768	99.999
Laumontite	-30.997	99.999	Microcline	-22.158	99.999	Magnetite	-34.370	99.999

Ca-Montmor.	-105.305	99.999	K-Montmor.	-52.289	99.999	Mg-Montmor.	-106.077	99.999
Na-Montmor.	-52.037	99.999	Muscovite	-25.971	99.999	Prehnite	-39.985	99.999
Pyrrhotite	-130.239	99.999	Pyrite	-194.028	99.999	Quartz	-3.751	99.999
Wairakite	-27.040	99.999	Wollastonite	13.028	99.999	Zoisite	-38.545	99.999
Epidote	-48.659	99.999	Marcasite	-166.147	99.999	Talc	20.206	99.999
Chrysotile	29.656	99.999	Sil. amorph.	-2.593	99.999			

Third step Aquifer liquid cooled to 30.0 øC

Deep water pH is 8.736

log solubility products of minerals in deep water

	Theor.	Calc.		Theor.	Calc.		Theor.	Calc.
Adularia	-20.950	99.999	Albite, low	-19.889	99.999	Analcime	-15.778	99.999
Anhydrite	-4.757	-5.158	Calcite	-8.528	-6.957	Chalcedony	-3.522	99.999
Mg-Chlorite	-84.696	99.999	Fluorite	-10.912	99.999	Goethite	-7.111	99.999
Laumontite	-31.845	99.999	Microcline	-22.925	99.999	Magnetite	-35.222	99.999
Ca-Montmor.	-109.392	99.999	K-Montmor.	-54.493	99.999	Mg-Montmor.	-110.080	99.999
Na-Montmor.	-54.178	99.999	Muscovite	-26.986	99.999	Prehnite	-40.778	99.999
Pyrrhotite	-135.548	99.999	Pyrite	-202.813	99.999	Quartz	-3.872	99.999
Wairakite	-27.596	99.999	Wollastonite	13.482	99.999	Zoisite	-39.238	99.999
Epidote	-49.684	99.999	Marcasite	-174.015	99.999	Talc	21.138	99.999
Chrysotile	30.911	99.999	Sil. amorph.	-2.670	99.999			

Third step Aquifer liquid cooled to 25.0 øC

Deep water pH is 8.804

log solubility products of minerals in deep water

	Theor.	Calc.		Theor.	Calc.		Theor.	Calc.
Adularia	-21.303	99.999	Albite, low	-20.211	99.999	Analcime	-16.023	99.999
Anhydrite	-4.709	-5.146	Calcite	-8.490	-6.925	Chalcedony	-3.583	99.999
Mg-Chlorite	-85.227	99.999	Fluorite	-10.966	99.999	Goethite	-7.286	99.999
Laumontite	-32.295	99.999	Microcline	-23.329	99.999	Magnetite	-35.665	99.999
Ca-Montmor.	-111.460	99.999	K-Montmor.	-55.612	99.999	Mg-Montmor.	-112.104	99.999
Na-Montmor.	-55.263	99.999	Muscovite	-27.506	99.999	Prehnite	-41.206	99.999
Pyrrhotite	-138.252	99.999	Pyrite	-207.357	99.999	Quartz	-3.933	99.999
Wairakite	-27.894	99.999	Wollastonite	13.720	99.999	Zoisite	-39.612	99.999
Epidote	-50.256	99.999	Marcasite	-178.077	99.999	Talc	21.623	99.999
Chrysotile	31.572	99.999	Sil. amorph.	-2.711	99.999			

ICELANDIC WATER CHEMISTRY GROUP Program WATCH, version 2.1 / 1994

Elguedri/1999 analysis

Om-Somaa-C.I.5

Water sample (mg/kg) Steam sample

pH/deg.C	6.60/ 25.0	Gas (volume %)		Reference temperature	deg.C : 70.9 (Measured)
CO2	252.46	CO2	.00		
H2S	.00	H2S	.00	Sampling pressure	bar abs. : 1.0
NH3	.00	NH3	.00	Discharge enthalpy	kJ/kg : 297. (Calculated)
B	.00	H2	.00	Discharge	kg/s : .0
SiO2	.00	O2	.00	Steam fraction at collection	: .0000
Na	388.53	CH4	.00		
K	54.74	N2	.00	Measured temperature	deg.C : 70.9
Mg	104.58				
Ca	188.38	Liters gas per kg			
F	.00	condensate/deg.C	.00/.0	Condensate (mg/kg)	
Cl	567.31			pH/deg.C	.00/ .0
SO4	561.95	Total steam (mg/kg)		CO2	.00
Al	.00	CO2	.00	H2S	.00
Fe	.00	H2S	.00	NH3	.00
TDS	1840.00	NH3	.00	Na	.00

Ionic strength = .04352
Ionic balance : Cations (mol.eq.) = .03366563 Anions (mol.eq.) =.02893033 Difference (%) = 15.13

Deep water pH is 6.508

log solubility products of minerals in deep water

	Theor.	Calc.		Theor.	Calc.		Theor.	Calc.
Adularia	-18.519	99.999	Albite, low	-17.669	99.999	Analcime	-14.089	99.999

Anhydrite	-5.216	-5.513	Calcite	-8.984	-8.892	Chalcedony	-3.090	99.999
Mg-Chlorite	-81.489	99.999	Fluorite	-10.618	99.999	Goethite	-5.716	99.999
Laumontite	-28.774	99.999	Microcline	-20.119	99.999	Magnetite	-31.919	99.999
Ca-Montmor.	-93.883	99.999	K-Montmor.	-46.148	99.999	Mg-Montmor.	-94.873	99.999
Na-Montmor.	-46.051	99.999	Muscovite	-23.177	99.999	Prehnite	-38.018	99.999
Pyrrhotite	-114.387	99.999	Pyrite	-168.871	99.999	Quartz	-3.396	99.999
Wairakite	-25.635	99.999	Wollastonite	11.795	99.999	Zoisite	-36.870	99.999
Epidote	-45.974	99.999	Marcasite	-143.476	99.999	Talc	17.641	99.999
Chrysotile	26.271	99.999	Sil. amorph.	-2.383	99.999			

First step Aquifer liquid cooled to 68.0 øC

Deep water pH is 6.508

log solubility products of minerals in deep water

	Theor.	Calc.		Theor.	Calc.		Theor.	Calc.
Adularia	-18.667	99.999	Albite, low	-17.804	99.999	Analcime	-14.191	99.999
Anhydrite	-5.180	-5.501	Calcite	-8.944	-8.892	Chalcedony	-3.117	99.999
Mg-Chlorite	-81.654	99.999	Fluorite	-10.631	99.999	Goethite	-5.816	99.999
Laumontite	-28.958	99.999	Microcline	-20.290	99.999	Magnetite	-32.142	99.999
Ca-Montmor.	-94.851	99.999	K-Montmor.	-46.669	99.999	Mg-Montmor.	-95.823	99.999
Na-Montmor.	-46.559	99.999	Muscovite	-23.412	99.999	Prehnite	-38.173	99.999
Pyrrhotite	-115.851	99.999	Pyrite	-171.130	99.999	Quartz	-3.427	99.999
Wairakite	-25.747	99.999	Wollastonite	11.901	99.999	Zoisite	-36.998	99.999
Epidote	-46.213	99.999	Marcasite	-145.522	99.999	Talc	17.863	99.999
Chrysotile	26.560	99.999	Sil. amorph.	-2.402	99.999			

Second step Aquifer liquid boiled to 67.0 øC Degassing coefficient is 1.0000

Deep water pH is 7.829

log solubility products of minerals in deep water

	Theor.	Calc.		Theor.	Calc.		Theor.	Calc.
Adularia	-18.718	99.999	Albite, low	-17.851	99.999	Analcime	-14.227	99.999
Anhydrite	-5.167	-5.500	Calcite	-8.930	-7.610	Chalcedony	-3.127	99.999
Mg-Chlorite	-81.713	99.999	Fluorite	-10.636	99.999	Goethite	-5.850	99.999
Laumontite	-29.023	99.999	Microcline	-20.350	99.999	Magnetite	-32.219	99.999
Ca-Montmor.	-95.190	99.999	K-Montmor.	-46.851	99.999	Mg-Montmor.	-96.155	99.999
Na-Montmor.	-46.737	99.999	Muscovite	-23.495	99.999	Prehnite	-38.227	99.999
Pyrrhotite	-116.357	99.999	Pyrite	-171.913	99.999	Quartz	-3.438	99.999
Wairakite	-25.787	99.999	Wollastonite	11.938	99.999	Zoisite	-37.044	99.999
Epidote	-46.296	99.999	Marcasite	-146.230	99.999	Talc	17.940	99.999
Chrysotile	26.661	99.999	Sil. amorph.	-2.408	99.999			

Second step Aquifer liquid boiled to 66.0 øC Degassing coefficient is 1.0000

Deep water pH is 8.084

log solubility products of minerals in deep water

	Theor.	Calc.		Theor.	Calc.		Theor.	Calc.
Adularia	-18.770	99.999	Albite, low	-17.899	99.999	Analcime	-14.263	99.999
Anhydrite	-5.155	-5.498	Calcite	-8.917	-7.385	Chalcedony	-3.136	99.999
Mg-Chlorite	-81.773	99.999	Fluorite	-10.641	99.999	Goethite	-5.885	99.999
Laumontite	-29.088	99.999	Microcline	-20.411	99.999	Magnetite	-32.297	99.999
Ca-Montmor.	-95.532	99.999	K-Montmor.	-47.035	99.999	Mg-Montmor.	-96.491	99.999
Na-Montmor.	-46.917	99.999	Muscovite	-23.578	99.999	Prehnite	-38.283	99.999
Pyrrhotite	-116.863	99.999	Pyrite	-172.699	99.999	Quartz	-3.449	99.999
Wairakite	-25.827	99.999	Wollastonite	11.976	99.999	Zoisite	-37.090	99.999
Epidote	-46.378	99.999	Marcasite	-146.941	99.999	Talc	18.018	99.999
Chrysotile	26.762	99.999	Sil. amorph.	-2.414	99.999			

Second step Aquifer liquid boiled to 65.0 øC Degassing coefficient is 1.0000

Deep water pH is 8.231

log solubility products of minerals in deep water

	Theor.	Calc.		Theor.	Calc.		Theor.	Calc.
Adularia	-18.823	99.999	Albite, low	-17.947	99.999	Analcime	-14.299	99.999
Anhydrite	-5.143	-5.496	Calcite	-8.904	-7.262	Chalcedony	-3.146	99.999
Mg-Chlorite	-81.834	99.999	Fluorite	-10.646	99.999	Goethite	-5.919	99.999
Laumontite	-29.154	99.999	Microcline	-20.472	99.999	Magnetite	-32.374	99.999
Ca-Montmor.	-95.877	99.999	K-Montmor.	-47.221	99.999	Mg-Montmor.	-96.829	99.999
Na-Montmor.	-47.098	99.999	Muscovite	-23.662	99.999	Prehnite	-38.339	99.999
Pyrrhotite	-117.369	99.999	Pyrite	-173.486	99.999	Quartz	-3.461	99.999
Wairakite	-25.868	99.999	Wollastonite	12.013	99.999	Zoisite	-37.137	99.999
Epidote	-46.461	99.999	Marcasite	-147.653	99.999	Talc	18.096	99.999
Chrysotile	26.865	99.999	Sil. amorph.	-2.421	99.999			

Second step Aquifer liquid boiled to 64.0 øC Degassing coefficient is 1.0000

Deep water pH is 8.335

log solubility products of minerals in deep water

	Theor.	Calc.		Theor.	Calc.		Theor.	Calc.
Adularia	-18.876	99.999	Albite, low	-17.995	99.999	Analcime	-14.336	99.999
Anhydrite	-5.130	-5.493	Calcite	-8.890	-7.178	Chalcedony	-3.156	99.999
Mg-Chlorite	-81.897	99.999	Fluorite	-10.651	99.999	Goethite	-5.953	99.999
Laumontite	-29.220	99.999	Microcline	-20.534	99.999	Magnetite	-32.451	99.999
Ca-Montmor.	-96.224	99.999	K-Montmor.	-47.408	99.999	Mg-Montmor.	-97.171	99.999
Na-Montmor.	-47.280	99.999	Muscovite	-23.747	99.999	Prehnite	-38.396	99.999
Pyrrhotite	-117.876	99.999	Pyrite	-174.276	99.999	Quartz	-3.472	99.999
Wairakite	-25.909	99.999	Wollastonite	12.051	99.999	Zoisite	-37.185	99.999
Epidote	-46.544	99.999	Marcasite	-148.367	99.999	Talc	18.175	99.999
Chrysotile	26.967	99.999	Sil. amorph.	-2.427	99.999			

Third step Aquifer liquid cooled to 60.0 øC

Deep water pH is 8.372

log solubility products of minerals in deep water

	Theor.	Calc.		Theor.	Calc.		Theor.	Calc.
Adularia	-19.092	99.999	Albite, low	-18.193	99.999	Analcime	-14.486	99.999
Anhydrite	-5.082	-5.477	Calcite	-8.839	-7.143	Chalcedony	-3.195	99.999
Mg-Chlorite	-82.157	99.999	Fluorite	-10.673	99.999	Goethite	-6.090	99.999
Laumontite	-29.492	99.999	Microcline	-20.784	99.999	Magnetite	-32.763	99.999
Ca-Montmor.	-97.642	99.999	K-Montmor.	-48.170	99.999	Mg-Montmor.	-98.562	99.999
Na-Montmor.	-48.023	99.999	Muscovite	-24.092	99.999	Prehnite	-38.631	99.999
Pyrrhotite	-119.909	99.999	Pyrite	-177.458	99.999	Quartz	-3.517	99.999
Wairakite	-26.078	99.999	Wollastonite	12.204	99.999	Zoisite	-37.383	99.999
Epidote	-46.879	99.999	Marcasite	-151.241	99.999	Talc	18.494	99.999
Chrysotile	27.386	99.999	Sil. amorph.	-2.453	99.999			

Third step Aquifer liquid cooled to 50.0 øC

Deep water pH is 8.471

log solubility products of minerals in deep water

	Theor.	Calc.		Theor.	Calc.		Theor.	Calc.
Adularia	-19.664	99.999	Albite, low	-18.715	99.999	Analcime	-14.883	99.999
Anhydrite	-4.966	-5.440	Calcite	-8.720	-7.064	Chalcedony	-3.297	99.999
Mg-Chlorite	-82.885	99.999	Fluorite	-10.737	99.999	Goethite	-6.429	99.999
Laumontite	-30.213	99.999	Microcline	-21.446	99.999	Magnetite	-33.553	99.999
Ca-Montmor.	-101.365	99.999	K-Montmor.	-50.170	99.999	Mg-Montmor.	-102.214	99.999
Na-Montmor.	-49.974	99.999	Muscovite	-25.002	99.999	Prehnite	-39.270	99.999
Pyrrhotite	-125.035	99.999	Pyrite	-185.595	99.999	Quartz	-3.632	99.999
Wairakite	-26.535	99.999	Wollastonite	12.603	99.999	Zoisite	-37.927	99.999
Epidote	-47.739	99.999	Marcasite	-158.572	99.999	Talc	19.326	99.999
Chrysotile	28.483	99.999	Sil. amorph.	-2.521	99.999			

Third step Aquifer liquid cooled to 40.0 øC

Deep water pH is 8.580

log solubility products of minerals in deep water

	Theor.	Calc.		Theor.	Calc.		Theor.	Calc.
Adularia	-20.282	99.999	Albite, low	-19.280	99.999	Analcime	-15.313	99.999
Anhydrite	-4.857	-5.407	Calcite	-8.616	-6.992	Chalcedony	-3.406	99.999
Mg-Chlorite	-83.730	99.999	Fluorite	-10.816	99.999	Goethite	-6.768	99.999
Laumontite	-30.997	99.999	Microcline	-22.158	99.999	Magnetite	-34.370	99.999
Ca-Montmor.	-105.305	99.999	K-Montmor.	-52.289	99.999	Mg-Montmor.	-106.077	99.999
Na-Montmor.	-52.037	99.999	Muscovite	-25.971	99.999	Prehnite	-39.985	99.999
Pyrrhotite	-130.239	99.999	Pyrite	-194.028	99.999	Quartz	-3.751	99.999
Wairakite	-27.040	99.999	Wollastonite	13.028	99.999	Zoisite	-38.545	99.999
Epidote	-48.659	99.999	Marcasite	-166.147	99.999	Talc	20.206	99.999
Chrysotile	29.656	99.999	Sil. amorph.	-2.593	99.999			

Third step Aquifer liquid cooled to 30.0 øC

Deep water pH is 8.699

log solubility products of minerals in deep water

	Theor.	Calc.		Theor.	Calc.		Theor.	Calc.
Adularia	-20.950	99.999	Albite, low	-19.889	99.999	Analcime	-15.778	99.999
Anhydrite	-4.757	-5.379	Calcite	-8.528	-6.929	Chalcedony	-3.522	99.999
Mg-Chlorite	-84.696	99.999	Fluorite	-10.912	99.999	Goethite	-7.111	99.999

Laumontite	-31.845	99.999	Microcline	-22.925	99.999	Magnetite	-35.222	99.999
Ca-Montmor.	-109.392	99.999	K-Montmor.	-54.493	99.999	Mg-Montmor.	-110.080	99.999
Na-Montmor.	-54.178	99.999	Muscovite	-26.986	99.999	Prehnite	-40.778	99.999
Pyrrhotite	-135.548	99.999	Pyrite	-202.813	99.999	Quartz	-3.872	99.999
Wairakite	-27.596	99.999	Wollastonite	13.482	99.999	Zoisite	-39.238	99.999
Epidote	-49.684	99.999	Marcasite	-174.015	99.999	Talc	21.138	99.999
Chrysotile	30.911	99.999	Sil. amorph.	-2.670	99.999			

Third step Aquifer liquid cooled to 25.0 øC

Deep water pH is 8.764

log solubility products of minerals in deep water

	Theor.	Calc.		Theor.	Calc.		Theor.	Calc.
Adularia	-21.303	99.999	Albite, low	-20.211	99.999	Analcime	-16.023	99.999
Anhydrite	-4.709	-5.366	Calcite	-8.490	-6.900	Chalcedony	-3.583	99.999
Mg-Chlorite	-85.227	99.999	Fluorite	-10.966	99.999	Goethite	-7.286	99.999
Laumontite	-32.295	99.999	Microcline	-23.329	99.999	Magnetite	-35.665	99.999
Ca-Montmor.	-111.460	99.999	K-Montmor.	-55.612	99.999	Mg-Montmor.	-112.104	99.999
Na-Montmor.	-55.263	99.999	Muscovite	-27.506	99.999	Prehnite	-41.206	99.999
Pyrrhotite	-138.252	99.999	Pyrite	-207.357	99.999	Quartz	-3.933	99.999
Wairakite	-27.894	99.999	Wollastonite	13.720	99.999	Zoisite	-39.612	99.999
Epidote	-50.256	99.999	Marcasite	-178.077	99.999	Talc	21.623	99.999
Chrysotile	31.572	99.999	Sil. amorph.	-2.711	99.999			

ICELANDIC WATER CHEMISTRY GROUP Program WATCH, version 2.1 / 1994

Elguedri/1999 analysis

Lymagues-C.I.8

Water sample (mg/kg) Steam sample

pH/deg.C	6.70/ 25.0	Gas (volume %)		Reference temperature deg.C :	72.5 (Measured)
CO2	124.07	CO2	.00		
H2S	.00	H2S	.00	Sampling pressure bar abs. :	1.0
NH3	.00	NH3	.00	Discharge enthalpy kJ/kg :	303. (Calculated)
B	.00	H2	.00	Discharge kg/s :	.0
SiO2	.00	O2	.00	Steam fraction at collection :	.0000
Na	287.00	CH4	.00		
K	36.00	N2	.00	Measured temperature deg.C :	72.5
Mg	103.00				
Ca	240.00	Liters gas per kg			
F	.00	condensate/deg.C	.00/.0	Condensate (mg/kg)	
Cl	497.00			pH/deg.C	.00/ .0
SO4	931.00	Total steam (mg/kg)		CO2	.00
Al	.00	CO2	.00	H2S	.00
Fe	.00	H2S	.00	NH3	.00
TDS	2450.00	NH3	.00	Na	.00

Ionic strength = .04633
Ionic balance : Cations (mol.eq.) = .02973192 Anions (mol.eq.) =.03132208 Difference (%) = -5.21

Deep water pH is 6.606

log solubility products of minerals in deep water

	Theor.	Calc.		Theor.	Calc.		Theor.	Calc.
Adularia	-18.439	99.999	Albite, low	-17.596	99.999	Analcime	-14.034	99.999
Anhydrite	-5.236	-5.213	Calcite	-9.006	-9.005	Chalcedony	-3.075	99.999
Mg-Chlorite	-81.401	99.999	Fluorite	-10.611	99.999	Goethite	-5.660	99.999
Laumontite	-28.675	99.999	Microcline	-20.026	99.999	Magnetite	-31.797	99.999
Ca-Montmor.	-93.359	99.999	K-Montmor.	-45.867	99.999	Mg-Montmor.	-94.359	99.999
Na-Montmor.	-45.776	99.999	Muscovite	-23.050	99.999	Prehnite	-37.935	99.999
Pyrrhotite	-113.581	99.999	Pyrite	-167.632	99.999	Quartz	-3.378	99.999
Wairakite	-25.574	99.999	Wollastonite	11.738	99.999	Zoisite	-36.801	99.999
Epidote	-45.843	99.999	Marcasite	-142.354	99.999	Talc	17.520	99.999
Chrysotile	26.113	99.999	Sil. amorph.	-2.374	99.999			

First step Aquifer liquid cooled to 70.0 øC

Deep water pH is 6.605

log solubility products of minerals in deep water

	Theor.	Calc.		Theor.	Calc.		Theor.	Calc.
Adularia	-18.565	99.999	Albite, low	-17.711	99.999	Analcime	-14.120	99.999
Anhydrite	-5.205	-5.204	Calcite	-8.971	-9.003	Chalcedony	-3.099	99.999
Mg-Chlorite	-81.539	99.999	Fluorite	-10.622	99.999	Goethite	-5.747	99.999
Laumontite	-28.831	99.999	Microcline	-20.171	99.999	Magnetite	-31.988	99.999

Ca-Montmor.	-94.181	99.999	K-Montmor.	-46.309	99.999	Mg-Montmor.	-95.165	99.999
Na-Montmor.	-46.207	99.999	Muscovite	-23.249	99.999	Prehnite	-38.065	99.999
Pyrrhotite	-114.841	99.999	Pyrite	-169.570	99.999	Quartz	-3.406	99.999
Wairakite	-25.669	99.999	Wollastonite	11.828	99.999	Zoisite	-36.909	99.999
Epidote	-46.048	99.999	Marcasite	-144.110	99.999	Talc	17.709	99.999
Chrysotile	26.360	99.999	Sil. amorph.	-2.389	99.999			

Second step Aquifer liquid boiled to 69.0 øC Degassing coefficient is 1.0000

Deep water pH is 7.875

log solubility products of minerals in deep water

	Theor.	Calc.		Theor.	Calc.		Theor.	Calc.
Adularia	-18.615	99.999	Albite, low	-17.757	99.999	Analcime	-14.155	99.999
Anhydrite	-5.192	-5.202	Calcite	-8.958	-7.780	Chalcedony	-3.108	99.999
Mg-Chlorite	-81.596	99.999	Fluorite	-10.627	99.999	Goethite	-5.782	99.999
Laumontite	-28.894	99.999	Microcline	-20.231	99.999	Magnetite	-32.065	99.999
Ca-Montmor.	-94.514	99.999	K-Montmor.	-46.488	99.999	Mg-Montmor.	-95.492	99.999
Na-Montmor.	-46.383	99.999	Muscovite	-23.330	99.999	Prehnite	-38.119	99.999
Pyrrhotite	-115.346	99.999	Pyrite	-170.349	99.999	Quartz	-3.416	99.999
Wairakite	-25.708	99.999	Wollastonite	11.865	99.999	Zoisite	-36.953	99.999
Epidote	-46.130	99.999	Marcasite	-144.815	99.999	Talc	17.786	99.999
Chrysotile	26.459	99.999	Sil. amorph.	-2.395	99.999			

Second step Aquifer liquid boiled to 68.0 øC Degassing coefficient is 1.0000

Deep water pH is 8.116

log solubility products of minerals in deep water

	Theor.	Calc.		Theor.	Calc.		Theor.	Calc.
Adularia	-18.667	99.999	Albite, low	-17.804	99.999	Analcime	-14.191	99.999
Anhydrite	-5.180	-5.198	Calcite	-8.944	-7.571	Chalcedony	-3.117	99.999
Mg-Chlorite	-81.654	99.999	Fluorite	-10.631	99.999	Goethite	-5.816	99.999
Laumontite	-28.958	99.999	Microcline	-20.290	99.999	Magnetite	-32.142	99.999
Ca-Montmor.	-94.851	99.999	K-Montmor.	-46.669	99.999	Mg-Montmor.	-95.823	99.999
Na-Montmor.	-46.559	99.999	Muscovite	-23.412	99.999	Prehnite	-38.173	99.999
Pyrrhotite	-115.851	99.999	Pyrite	-171.130	99.999	Quartz	-3.427	99.999
Wairakite	-25.747	99.999	Wollastonite	11.901	99.999	Zoisite	-36.998	99.999
Epidote	-46.213	99.999	Marcasite	-145.522	99.999	Talc	17.863	99.999
Chrysotile	26.560	99.999	Sil. amorph.	-2.402	99.999			

Second step Aquifer liquid boiled to 67.0 øC Degassing coefficient is 1.0000

Deep water pH is 8.254

log solubility products of minerals in deep water

	Theor.	Calc.		Theor.	Calc.		Theor.	Calc.
Adularia	-18.718	99.999	Albite, low	-17.851	99.999	Analcime	-14.227	99.999
Anhydrite	-5.167	-5.195	Calcite	-8.930	-7.457	Chalcedony	-3.127	99.999
Mg-Chlorite	-81.713	99.999	Fluorite	-10.636	99.999	Goethite	-5.850	99.999
Laumontite	-29.023	99.999	Microcline	-20.350	99.999	Magnetite	-32.219	99.999
Ca-Montmor.	-95.190	99.999	K-Montmor.	-46.851	99.999	Mg-Montmor.	-96.155	99.999
Na-Montmor.	-46.737	99.999	Muscovite	-23.495	99.999	Prehnite	-38.227	99.999
Pyrrhotite	-116.357	99.999	Pyrite	-171.913	99.999	Quartz	-3.438	99.999
Wairakite	-25.787	99.999	Wollastonite	11.938	99.999	Zoisite	-37.044	99.999
Epidote	-46.296	99.999	Marcasite	-146.230	99.999	Talc	17.940	99.999
Chrysotile	26.661	99.999	Sil. amorph.	-2.408	99.999			

Second step Aquifer liquid boiled to 66.0 øC Degassing coefficient is 1.0000

Deep water pH is 8.352

log solubility products of minerals in deep water

	Theor.	Calc.		Theor.	Calc.		Theor.	Calc.
Adularia	-18.770	99.999	Albite, low	-17.899	99.999	Analcime	-14.263	99.999
Anhydrite	-5.155	-5.191	Calcite	-8.917	-7.379	Chalcedony	-3.136	99.999
Mg-Chlorite	-81.773	99.999	Fluorite	-10.641	99.999	Goethite	-5.885	99.999
Laumontite	-29.088	99.999	Microcline	-20.411	99.999	Magnetite	-32.297	99.999
Ca-Montmor.	-95.532	99.999	K-Montmor.	-47.035	99.999	Mg-Montmor.	-96.491	99.999
Na-Montmor.	-46.917	99.999	Muscovite	-23.578	99.999	Prehnite	-38.283	99.999
Pyrrhotite	-116.863	99.999	Pyrite	-172.699	99.999	Quartz	-3.449	99.999
Wairakite	-25.827	99.999	Wollastonite	11.976	99.999	Zoisite	-37.090	99.999
Epidote	-46.378	99.999	Marcasite	-146.941	99.999	Talc	18.018	99.999
Chrysotile	26.762	99.999	Sil. amorph.	-2.414	99.999			

Second step Aquifer liquid boiled to 65.0 øC Degassing coefficient is 1.0000

Deep water pH is 8.429

log solubility products of minerals in deep water

	Theor.	Calc.		Theor.	Calc.		Theor.	Calc.
Adularia	-18.823	99.999	Albite, low	-17.947	99.999	Analcime	-14.299	99.999
Anhydrite	-5.143	-5.187	Calcite	-8.904	-7.320	Chalcedony	-3.146	99.999
Mg-Chlorite	-81.834	99.999	Fluorite	-10.646	99.999	Goethite	-5.919	99.999
Laumontite	-29.154	99.999	Microcline	-20.472	99.999	Magnetite	-32.374	99.999
Ca-Montmor.	-95.877	99.999	K-Montmor.	-47.221	99.999	Mg-Montmor.	-96.829	99.999
Na-Montmor.	-47.098	99.999	Muscovite	-23.662	99.999	Prehnite	-38.339	99.999
Pyrrhotite	-117.369	99.999	Pyrite	-173.486	99.999	Quartz	-3.461	99.999
Wairakite	-25.868	99.999	Wollastonite	12.013	99.999	Zoisite	-37.137	99.999
Epidote	-46.461	99.999	Marcasite	-147.653	99.999	Talc	18.096	99.999
Chrysotile	26.865	99.999	Sil. amorph.	-2.421	99.999			

Third step Aquifer liquid cooled to 60.0 øC

Deep water pH is 8.481

log solubility products of minerals in deep water

	Theor.	Calc.		Theor.	Calc.		Theor.	Calc.
Adularia	-19.092	99.999	Albite, low	-18.193	99.999	Analcime	-14.486	99.999
Anhydrite	-5.082	-5.170	Calcite	-8.839	-7.271	Chalcedony	-3.195	99.999
Mg-Chlorite	-82.157	99.999	Fluorite	-10.673	99.999	Goethite	-6.090	99.999
Laumontite	-29.492	99.999	Microcline	-20.784	99.999	Magnetite	-32.763	99.999
Ca-Montmor.	-97.642	99.999	K-Montmor.	-48.170	99.999	Mg-Montmor.	-98.562	99.999
Na-Montmor.	-48.023	99.999	Muscovite	-24.092	99.999	Prehnite	-38.631	99.999
Pyrrhotite	-119.909	99.999	Pyrite	-177.458	99.999	Quartz	-3.517	99.999
Wairakite	-26.078	99.999	Wollastonite	12.204	99.999	Zoisite	-37.383	99.999
Epidote	-46.879	99.999	Marcasite	-151.241	99.999	Talc	18.494	99.999
Chrysotile	27.386	99.999	Sil. amorph.	-2.453	99.999			

Third step Aquifer liquid cooled to 50.0 øC

Deep water pH is 8.592

log solubility products of minerals in deep water

	Theor.	Calc.		Theor.	Calc.		Theor.	Calc.
Adularia	-19.664	99.999	Albite, low	-18.715	99.999	Analcime	-14.883	99.999
Anhydrite	-4.966	-5.137	Calcite	-8.720	-7.181	Chalcedony	-3.297	99.999
Mg-Chlorite	-82.885	99.999	Fluorite	-10.737	99.999	Goethite	-6.429	99.999
Laumontite	-30.213	99.999	Microcline	-21.446	99.999	Magnetite	-33.553	99.999
Ca-Montmor.	-101.365	99.999	K-Montmor.	-50.170	99.999	Mg-Montmor.	-102.214	99.999
Na-Montmor.	-49.974	99.999	Muscovite	-25.002	99.999	Prehnite	-39.270	99.999
Pyrrhotite	-125.035	99.999	Pyrite	-185.595	99.999	Quartz	-3.632	99.999
Wairakite	-26.535	99.999	Wollastonite	12.603	99.999	Zoisite	-37.927	99.999
Epidote	-47.739	99.999	Marcasite	-158.572	99.999	Talc	19.326	99.999
Chrysotile	28.483	99.999	Sil. amorph.	-2.521	99.999			

Third step Aquifer liquid cooled to 40.0 øC

Deep water pH is 8.710

log solubility products of minerals in deep water

	Theor.	Calc.		Theor.	Calc.		Theor.	Calc.
Adularia	-20.282	99.999	Albite, low	-19.280	99.999	Analcime	-15.313	99.999
Anhydrite	-4.857	-5.108	Calcite	-8.616	-7.101	Chalcedony	-3.406	99.999
Mg-Chlorite	-83.730	99.999	Fluorite	-10.816	99.999	Goethite	-6.768	99.999
Laumontite	-30.997	99.999	Microcline	-22.158	99.999	Magnetite	-34.370	99.999
Ca-Montmor.	-105.305	99.999	K-Montmor.	-52.289	99.999	Mg-Montmor.	-106.077	99.999
Na-Montmor.	-52.037	99.999	Muscovite	-25.971	99.999	Prehnite	-39.985	99.999
Pyrrhotite	-130.239	99.999	Pyrite	-194.028	99.999	Quartz	-3.751	99.999
Wairakite	-27.040	99.999	Wollastonite	13.028	99.999	Zoisite	-38.545	99.999
Epidote	-48.659	99.999	Marcasite	-166.147	99.999	Talc	20.206	99.999
Chrysotile	29.656	99.999	Sil. amorph.	-2.593	99.999			

Third step Aquifer liquid cooled to 30.0 øC

Deep water pH is 8.839

log solubility products of minerals in deep water

	Theor.	Calc.		Theor.	Calc.		Theor.	Calc.
Adularia	-20.950	99.999	Albite, low	-19.889	99.999	Analcime	-15.778	99.999
Anhydrite	-4.757	-5.083	Calcite	-8.528	-7.030	Chalcedony	-3.522	99.999
Mg-Chlorite	-84.696	99.999	Fluorite	-10.912	99.999	Goethite	-7.111	99.999
Laumontite	-31.845	99.999	Microcline	-22.925	99.999	Magnetite	-35.222	99.999
Ca-Montmor.	-109.392	99.999	K-Montmor.	-54.493	99.999	Mg-Montmor.	-110.080	99.999
Na-Montmor.	-54.178	99.999	Muscovite	-26.986	99.999	Prehnite	-40.778	99.999

Pyrrhotite	-135.548	99.999	Pyrite	-202.813	99.999	Quartz	-3.872	99.999
Wairakite	-27.596	99.999	Wollastonite	13.482	99.999	Zoisite	-39.238	99.999
Epidote	-49.684	99.999	Marcasite	-174.015	99.999	Talc	21.138	99.999
Chrysotile	30.911	99.999	Sil. amorph.	-2.670	99.999			

Third step Aquifer liquid cooled to 25.0 øC

Deep water pH is 8.907

log solubility products of minerals in deep water

	Theor.	Calc.		Theor.	Calc.		Theor.	Calc.
Adularia	-21.303	99.999	Albite, low	-20.211	99.999	Analcime	-16.023	99.999
Anhydrite	-4.709	-5.072	Calcite	-8.490	-6.999	Chalcedony	-3.583	99.999
Mg-Chlorite	-85.227	99.999	Fluorite	-10.966	99.999	Goethite	-7.286	99.999
Laumontite	-32.295	99.999	Microcline	-23.329	99.999	Magnetite	-35.665	99.999
Ca-Montmor.	-111.460	99.999	K-Montmor.	-55.612	99.999	Mg-Montmor.	-112.104	99.999
Na-Montmor.	-55.263	99.999	Muscovite	-27.506	99.999	Prehnite	-41.206	99.999
Pyrrhotite	-138.252	99.999	Pyrite	-207.357	99.999	Quartz	-3.933	99.999
Wairakite	-27.894	99.999	Wollastonite	13.720	99.999	Zoisite	-39.612	99.999
Epidote	-50.256	99.999	Marcasite	-178.077	99.999	Talc	21.623	99.999
Chrysotile	31.572	99.999	Sil. amorph.	-2.711	99.999			

APPENDIX III: A 1 ¼" corrosion coupon holder of the type used in Iceland